Abstract

TANG, YINGJIE. Electron Emission Spectroscopy Characterization of N-doped Diamond and Si-doped AlGaN. (Under the direction of Dr. Robert J. Nemanich.)

Semiconductors with negative electron affinity provide an alternative way to achieve low work function materials because the Fermi level could be increased in the band gap by the process and doping engineering, while the surface termination will maintain the vacuum level below the conduction band minimum.

Thermionic emission and ultraviolet photoemission spectroscopy (UPS) were employed to determine the temperature dependent electron emission energy distribution from nitrogen doped diamond films prepared by microwave plasma chemical vapor deposition (CVD). The photoemission spectra obtained at room temperature indicated a work function of 1.8eV and a negative electron affinity (NEA). The thermionic emission and photoemission spectra obtained at 380°C indicated a minimum kinetic energy of 1.5eV relative to the Fermi level. Both spectra displayed the same sharp cutoff corresponding to the conduction band minimum (CBM). The temperature dependence of the Fermi energy and the surface band bending were modeled to account for the work function reduction with increased temperature. The increased binding energy of the VBM (3.7eV) and the C1s core level (286.6eV) were indications of the increase of the Fermi level within the bandgap.

The difference of surface band bending for the CVD diamond in comparison with results for natural single diamond was discussed regarding the donor and acceptor surface state. A band diagram was proposed to describe the electron transport and thermionic emission process for the N-doped diamond thin film

structure. The coupling of the sp2 and sp3 bonded carbon appears to play an important role in the electron transport.

The thermionic emission properties of both Dysprosium and N-doped CVD diamond with a negative electron affinity (NEA) were investigated with thermionic emission spectroscopy (TES). At a temperature of 370oC thermionic emission from N-doped diamond was observed with a minimum kinetic energy of 2.5eV relative to the Fermi level, while thermionic emission from Dy was detected until temperature above 560OC with 2.5eV work Function. The different thermionic emission properties between N-doped diamond and Dy were attributed to the negative electron affinity (NEA) on diamond surface. Fitting results showed thermionic emission from Dy follows the traditional Maxwell-Boltzmann distribution while the thermionic emission CVD diamond is more close to the half-Maxwellian distribution.

N-polar and Al (Ga)-polar AlGaN films were grown on C-polar and Si-polar SiC substrates, respectively. Atomic Force Microscopy images of the surfaces after KOH etching verified the N-polar face which is highly reactive and showed etch pits while the Al-face was resistant to KOH etching. Combined XPS and UPS characterization have shown that both N-polar and Al-polar surfaces of AlN have a zero or negative electron affinity. Furthermore, it has been determined that the N-face AlN has a lower work function (2.5eV) than the Al-face AlN (3.0 eV). The difference is attributed to the spontaneous polarization field. The results for the AlGaN alloy surfaces indicate that as the Al concentration is increased, the electron affinity and work function decreases.

Electron Emission Spectroscopy Characterization of N-doped Diamond and Si-doped AlGaN

By

YINGJIE TANG

A dissertation submitted to the Graduate Faculty
of North Carolina State University in partial fulfillment
of the requirements for the degree of Doctor of
Philosophy

PHYSICS

Raleigh, NC

2007

APPROVED BY:

_____	_____
R.J. Nemanich, Chair of Advisory Committee	Z.S. Sitar
_____	_____
H.D. Hallen	T. P. Pear

Biography

Yingjie Tang was born in Qingdao, China on July 7th, 1977. In 1995, he entered Shangdong University, Jinan, China. He majored in physics and received his B. S. degree in 1999. Then, he was admitted to Peking University to study nitride semiconductors and white light emitting diodes, and received his MS in physics in 2002. Motivated to pursue a Ph.D. degree, he joined in the Surface Science lab at North Carolina State University, Raleigh, NC. Under the direction of Dr. Nemanich, he has developed a deep understanding of material physics which in turn has been activating him significant interest in this area.

Acknowledgements

I would like to sincerely thank my advisor, my advisory committee chair, Dr. Nemanich for his continuous encouragement, intelligent guidance, invaluable support, and friendship throughout my study and research at North Carolina State University. I would like to thank Dr. Sitar, Dr. Hallen and Dr. Pearl for the support, encouragement and serving in my advisory committee

I would like to especially thank Franz Köeck, Ji-Soo Park and Charlie Fulton for their help and support in my research at Surface Science Lab.

I would also like to show my appreciation to Eugene Bryan, Anderson Sunda-Meya, Matthew Zeman, Matt Brukman, Jiyoung Choung, Jacob Garguilo, Jacquie Hanson, Wendy Kong, Xin Li, Jeff Mullen, James Perkins, Joshua Smith, Anderson Sunda-Meya, Leigh Winfrey, Brian Rodriguez, John Waldrep, Thomas Blair, James Burnette, Will Mecouch and Yunyu Wang.

I would like to sincerely thank my parents, Yunrui Tang and Li Zhou for their love, support and encouragement for my education; my wife Xiang Zhou for sharing me the pain and happiness over the years; and my son Jason Tang for his coming and giving me responsibility and motivation to move forward.

Table of Contents

List of Figures

1. Introduction

1.1 Motivation

The work function of a material is defined as the difference between the Fermi energy level and the vacuum energy level[1]. It is a fundamental parameter for the investigations of vacuum thermionic emission as well as the metal-semiconductor junction in solid state devices. The thermionic emission has applications in cathode/X-ray tubes, gauges, mass spectrometers, electron microscopes as well as energy conversion. However, one of the difficulties in the device engineering for more applications was to achieve the lower work function materials. In all elements, most metals have work functions between 3eV and 6eV and Cesium (Cs) has the lowest work function, 1.7eV. However, the disadvantage of Cs material is its reactivity with the surrounding or contact material and Cs could melt/evaporate at the high temperature (>300^{o}C) conditions.

A thermionic converter, shown in Fig 1.1, is a device that converts heat directly into electric power by thermionic electron emission. Electrons are emitted from a hot electrode and collected by a colder electrode.

Semiconductors with negative electron affinity provide an alternative way to achieve low work function materials because the Fermi level could be increased in the band gap by the process and doping engineering, while the surface termination will maintain the vacuum level below the conduction band minimum. In a semiconductor, the electron affinity is the difference between the vacuum energy level and the conduction band minimum. The term negative electron affinity (NEA) refers to the condition where the vacuum level lies below the conduction band minimum. An electron with an energy greater than or equal to the conduction band minimum can

escape into vacuum without an energy barrier at the surface of the semiconductor. Thus, an NEA surface may be expected to enhance cathode emission. Fig 1.2 shows the band diagram of an n-type semiconductor with a negative electron affinity.

The work function of the material is very sensitive to the materials surface conditions, such as absorbed or evaporated layers, surface reconstruction, surface charging, oxide layer imperfections, surface and bulk contamination, etc.

1.2 Diamond and Nitride semiconductors

The materials of interest are diamond, aluminum nitride, and aluminum gallium nitride alloys. These materials have properties of negative/low electron affinity[2-4] and high thermal conductivity, which meet the requirements of device design. The large bandgaps and significant high-field electron mobilities also make these materials candidates for high-power vacuum microelectronic applications[5].

Diamond with a band gap of 5.47 eV is known to exhibit a negative electron affinity on (111) and (001) surfaces with hydrogen termination[6]. The surface terminations can shift the position of the bands with respect to the vacuum level. In Fig 1.3, the electron affinity of diamond may vary from -1.2 eV for the fully hydrogenated C (001) - (2 x1):H up to +1.7 eV for the oxidized C (001) -(1 x1):O surface due to the formation of a surface dipole[3, 6-8]. The lone pair orbitals of polar C-O bond extending from the surface are expected to increase the work function[8]. In contrast, C-H bonds are relatively nonpolar due to the similar electronegativities of C and H and the monohydride terminated surface relaxes to a 2x1 reconstructed surface., resulting in a dipole such that work function is reduced compared to the oxidized or clean diamond surface.

Nitrogen is a common impurity in both natural and CVD diamond. It is a deep donor in diamond with a level typically assigned at 1.7 eV[9] below the conduction band minimum, shown in Fig 1.3. Nitrogen-doped diamond films were prepared on 25 mm-diameter polished molybdenum substrates by microwave plasma-assisted chemical vapor deposition using a three-step growth method.

The III-nitrides occur primarily in the wurzite crystal structure. It have been shown that wurtzite AlN grown on polar (0001)/(000-1) 6-H SiC surface presents low or negative electron affinity (NEA)[2, 4]. The spontaneous polarization along <0001>, shown in Fig 4 (a), is an inherent characteristic of the III-nitride compounds[10]. The [0001] axis points from the N-face to the III-face. The gradient in the polarization induces bound surface charges so that the energy bands at the surface are modified. For epitaxial layers of III-nitrides with metal-face polarity, the bound surface charge is negative, whereas for N-face III-nitrides the bound surface charge is positive. As a result, metal polar surface, exhibit higher surface energy barrier than the N-polar surface because of surface band bending. The free electrons in the nitride material will screen the polarization bound charges at surface, resulting in the formation of depletion/accumulation layer at Ga or N polar surface, indicated in the W. C. Yang's work[11]. Fig 4 (b) shows band diagram of III-nitrides with built-in polarization field.

1.3 Photoemission and thermionic emission

The work function of a material may be determined from the thermionic emission, the photoelectron emission, the contact potential difference and the field emission. Photoelectron emission is more widely accepted as a direct method for work function determination.

Photoemission spectroscopy is an application of the photoelectric effect. The process has been described using a three-step model[1]: 1) excitation of electrons into states in the conduction band, 2) propagation of the electrons to the surface and generation of secondary electrons, and 3) emission of electrons into vacuum. Photoemission spectroscopy is a surface sensitive technique due to the short mean free path (<30 Å) of low energy electrons.

X-ray photoelectron spectroscopy (XPS) employs X-rays as the photon source, with sources being magnesium (hν=1253.6 eV) and aluminum (hν=1486.6 eV). XPS is often employed to investigate the chemical properties of surfaces, by observation of core level characteristics of the material. The binding energy (BE) is related to the kinetic energy of the emitted electron by BE=*hν*-KE-Φ, where *hν* is the energy of the photon, KE is the kinetic energy of the electron and Φ is the material work function. A value of zero binding energy is the Fermi level.

Ultraviolet photoelectron spectroscopy employs UV light generated from a gas discharge lamp. The most common gas used to generate such light is helium with discharge energies He I (hν=21.2 eV) and He II (hν=40.8 eV). Angle resolved ultraviolet photoemission spectroscopy (ARUPS) can be used to investigate the valence band electronic states because the intensity of the signal reflects the density of states in the valence band.

Ultraviolet photoemission spectroscopy (UPS) also allows for the measurement of the electron affinity of semiconductor and the work function of metal. Fig 1.5 displays the principle of determination of electron affinity of semiconductor by ultraviolet photoemission spectroscopy. The semiconductor electron affinity (χ) and work function (Φ) are given by $\chi = h\nu - W - Eg$ and $\Phi = h\nu - W - VBM$, where *hν* is the energy of the photon, the W represents the width of the spectra, Eg is the band gap

and VBM is the valence band maxim referenced with the Fermi level. For NEA semiconductors, the sharp peak at low kinetic electron energies represents the energy position of the conduction band minimum. The vacuum level is below the conduction band minimum and the exact position of the vacuum level can not be determined by UPS alone.

Thermionic emission is described by the Richardson equation[12, 13] that the emitted current density J is related to temperature T, as $J=AT^2\exp(-\Phi/k_BT)$, where A is the Richarson constant, T is absolute temperature, Φ is the work function and k_B is the Boltzmann constant. Thermionic emission spectroscopy[14, 15] can be employed to investigate the work function, the energy distribution and the transport properties of emitter materials at high temperature. The energy distribution P(E) follows the Maxwell-Boltzmann distribution as $P(E) = dj/dE = C * E * \exp[-\frac{E}{k_B T}]$, where C is constant, E is the kinetic energy of the electrons, T is absolute temperature and k_B is the Boltzmann constant. However, Hutson[14] in his work showed thermionic emission with an $E^{1/2}\exp(-E/k_BT)$ distribution.

1.4 Outline of the thesis

Chapter 2 introduced the experiment of temperature dependent photoemission and thermionic emission spectroscopy. Chapter 3 describes the thermionic emission from low work function N-doped CVD diamond films. Chapter 4 investigates the negative electron affinity effect on the thermionic emission from N-doped Diamond. Chapter 5 discussed the energy distribution of thermionic emission from nitrogen-doped diamond. Chapter 6 studies the polarity effect on the surface electronic properties of AlGaN. Chapter 7 presents conclusion of the work and future directions for the research.

1.5 References

[1] M. Cardona and L. Ley, *Photoemission in Solids I* (Springer, 1978).

[2] M. C. Benjamin, C. Wang, R. F. Davis, and R. J. Nemanich, Appl. Phys. Lett. **64**, 3288 (1994).

[3] J. Vanderweide, Z. Zhang, P. K. Baumann, M. G. Wensell, J. Bernholc, and R. J. Nemanich, Phys. Rev. B **50**, 5803 (1994).

[4] S. P. Grabowski, M. Schneider, H. Nienhaus, W. Monch, R. Dimitrov, O. Ambacher, and M. Stutzmann, Appl. Phys. Lett. **78**, 2503 (2001).

[5] V. V. Zhirnov, G. J. Wojak, W. B. Choi, J. J. Cuomo, and J. J. Hren, J. Vac. Sci. Technol. A-Vac. Surf. Films **15**, 1733 (1997).

[6] P. K. Baumann and R. J. Nemanich, Surf. Sci. **409**, 320 (1998).

[7] J. Robertson and M. J. Rutter, Diam. Relat. Mat. **7**, 620 (1998).

[8] J. Robertson, Diam. Relat. Mat. **5**, 797 (1996).

[9] R. G. Farrer, Solid State Commun. **7**, 685 (1969).

[10] O. Ambacher, et al., J. Appl. Phys. **85**, 3222 (1999).

[11] W. C. Yang, B. J. Rodriguez, M. Park, R. J. Nemanich, O. Ambacher, and V. Cimalla, J. Appl. Phys. **94**, 5720 (2003).

[12] C. Herring and M. H. Nichols, Rev. Mod. Phys. **21**, 185 (1949).

[13] E. B. Hensley, J. Appl. Phys. **32**, 301 (1961).

[14] A. R. Hutson, Phys. Rev. **98**, 889 (1955).

[15] V. S. Robinson, T. S. Fisher, J. A. Michel, and C. M. Lukehart, Appl. Phys. Lett. **87** (2005).

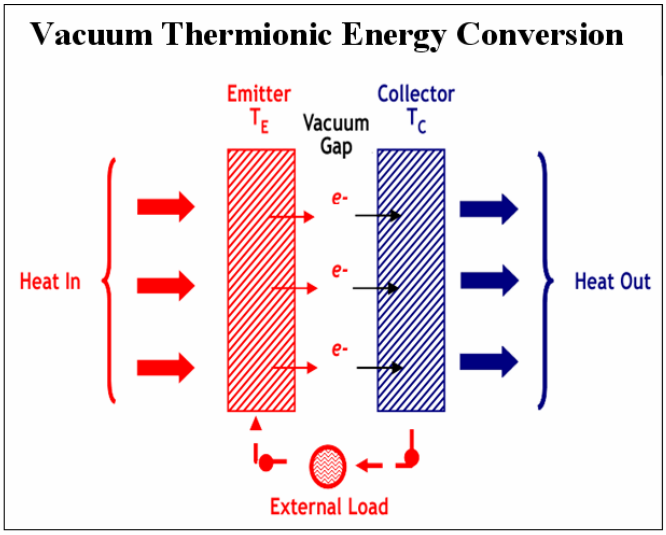

Fig 1.1 Thermionic energy conversion device that converts heat directly into electric power by thermionic electron emission.

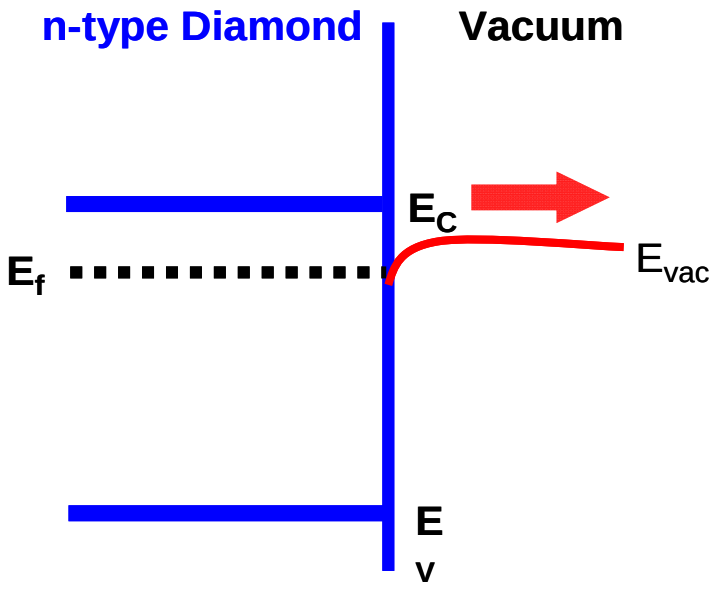

Fig 1.2 the band diagram of n-type semiconductor with negative electron affinity.

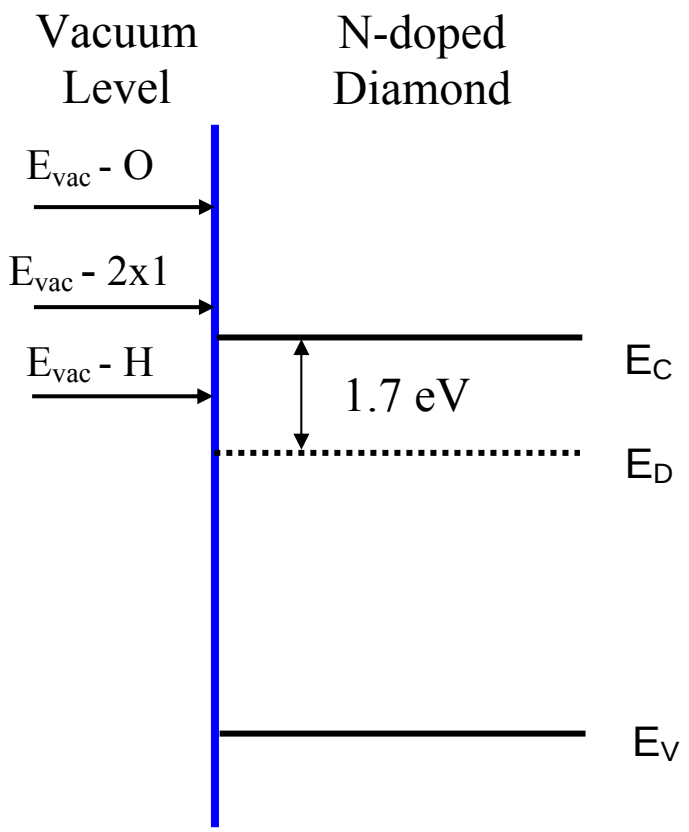

Fig 1.3 the electron affinity of diamond may vary from -1.2 eV for the fully hydrogenated C (001) - (2 x1):H up to +1.7 eV for the oxidized C (001) -(1 x1):O surface

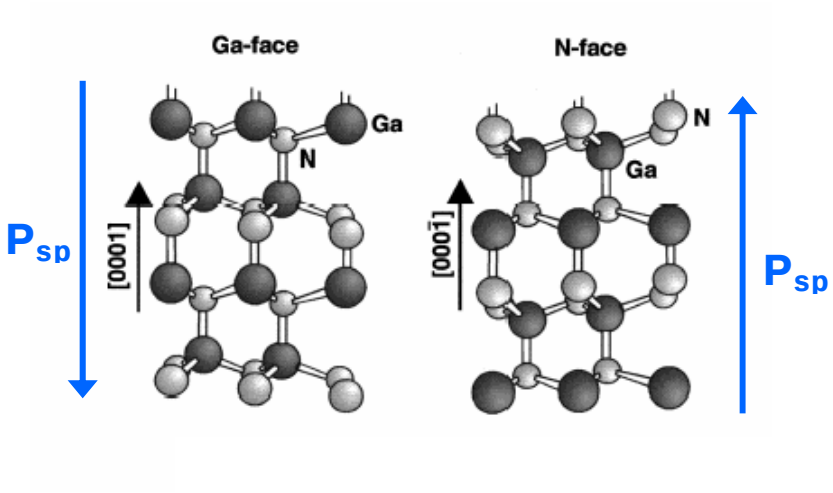

(a)

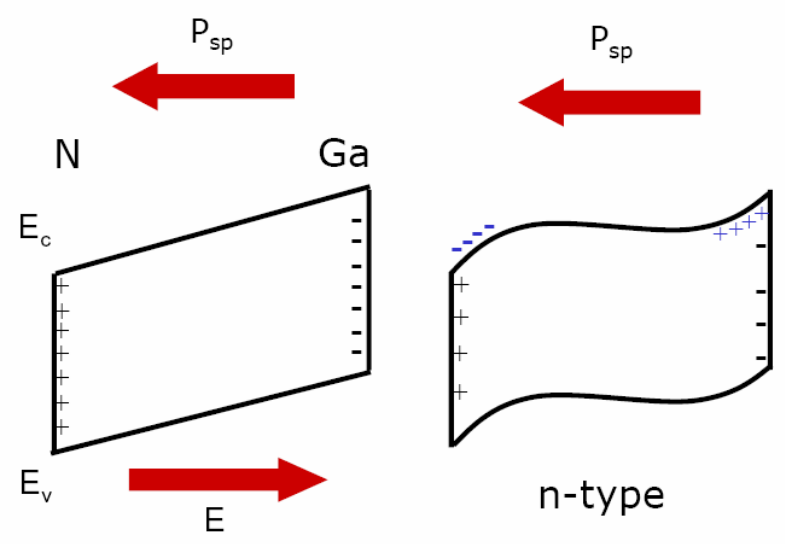

(b)

Figure 1.4 III-nitrides has (a) wurzite crystal structure.with the spontaneous polarization along <0001> (Ambacher, J. Appl. Phys. 85 (1999)). (b) Upward band bending at Ga-polar surface and downward band bending at N-polar surface. Left part shows built-in polarization field only. The surface bound charge is screened by the ionized donors, shown in the right diagram.

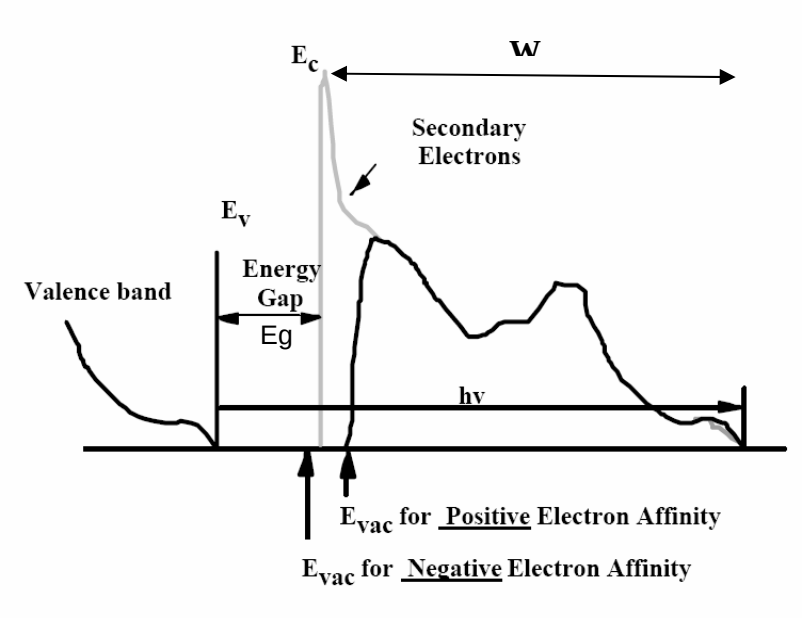

Fig 1.5 Principle of determination of electron affinity of semiconductor by ultraviolet photoemission spectroscopy[2] (Benjamin, Appl. Phys. Lett. **64**, 3288 (1994)).

2. Equipment and Experiment: temperature dependent UV photoemission and thermionic emission spectroscopy

The temperature dependent UV-photoemission spectroscopy and thermionic emission spectroscopy measurements were carried out in the same UHV chamber with a base pressure of ~$3x10^{-10}$ Torr. Ultraviolet photoelectron spectra were obtained with He I (21.2eV) radiation from an Omicron HIS13 discharge lamp, and the emitted electrons were measured with a VSW-HA50 hemispherical analyzer operating at a resolution of 0.1 eV. Thermionic emission spectra can be obtained with the same VSW-HA50 electron analyzer without UV excitation. The elevated sample temperature in the spectroscopy measurements was achieved by radiative heating from a tungsten coil filament mounted on a boron nitride disk behind the sample.

In Fig 2.1(a), the heater, made by a 0.5mm diameter tungsten wire formed in a coil shape, is mounted on a boron nitride insulating plate connected to the sample manipulator stage in the system. A K-type thermocouple is then placed in the center of the coil to measure the temperature. The average distance between the sample/plate back and the heater coil is 0.5cm. The heaters are controlled using Eurotherm 818 controllers/programmers connected to Eurotherm 831 SCR solid-state relays. A chromel–alumnel (K-type) thermocouple as well as optical pyrometer (MIKRON-M90Q) was employed to measure the sample surface temperature for temperatures above 250°C. Temperature measurements below 250°C were obtained by linear extrapolation of the thermocouple-pyrometer calibration curve. The thermocouple measures the temperature and returns the signal to the Eurotherm 818, then the 818 sends a signal to the 831, which outputs a current to the heater coil. This loop continues until the desired temperature is achieved.

The VSW HA50 (50mm radius, 4-element lens) hemispherical analyzer in Fig 2.1(b), is employed to measure the kinetic energy of photoemission electrons as well as thermionic electrons. A VSW HAC300 high-resolution control unit drives the analyzer and is connected to a Stanford Research Systems SR400 two channel gated photon counter with energy measurement range of 100eV. When the VSW HA50 hemispherical analyzer was used to investigate the peak energy and shape of the electron energy distribution, it is necessary to consider the instrument effect on the measurement. The peak width refers to the full width at half maximum (FWHM) of a specific peak. The natural peak will be broadening by the convolution with the Gaussian function of the analyzer.

It is noted that the electromagnetic field from the coil heater could possibly affect the spectroscopy. For the solenoid with infinite length, the magnetic flux is always kept inside and the outside magnetic/electric field is zero for either AC or DC condition. In the similar case, the ideal round and enclosed solenoid also keep the outside magnetic field zero due to the Ampere's law. Our round and enclosed solenoid heater did not showed any effect on the Fermi level position with the gold surface temperature up to 600ºC when the Fermi level of the analyzer was calibrated by the clean gold surface at elevated temperature. The temperature limit of 600 ºC for experiments is to protect the analyzer, 2cm in front of the sample, not be heated. The sample could keep the surface temperature at 320-350ºC for more than 1 min when the heater was off at 350ºC. The UV photoemission or thermionic spectroscopy of N-doped CVD diamond with the heater off didn't showed any change compared with the spectroscopy with heater on at 320-350ºC.

The thermionic emission spectroscopy has been employed to study the N-doped CVD diamond, a dysprosium film and a sample of a patterned N-dope diamond tip

array. The TES with temperature up to 600ºC could be detected only for materials with work function below 3eV. N-doped CVD diamond and Dy will be discussed in chapters 2 and 5.

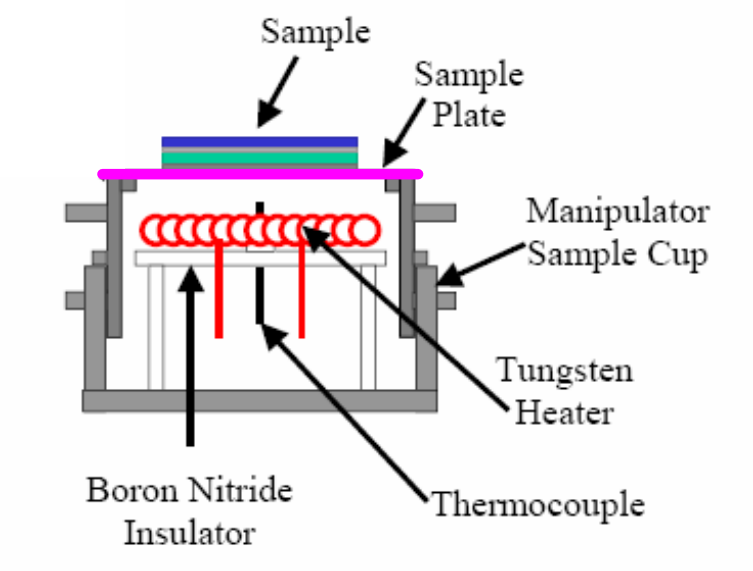

(a)

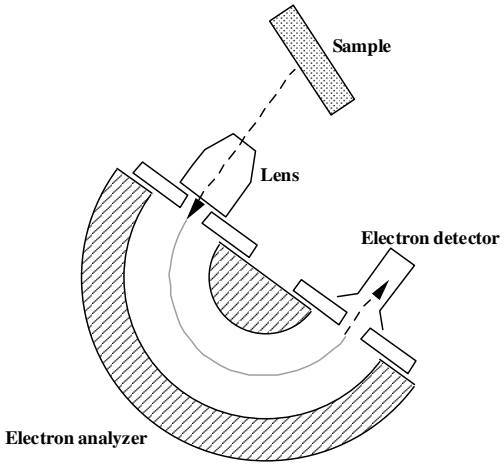

(b)

Fig 2.1 Thermionic emission spectroscopy includes (a) round and enclosed solenoid heater (b) VSW HA50 hemispherical analyzer

3. Thermionic emission from low work function N-doped CVD diamond films

Yingjie Tang, Franz A. M. Koeck and Robert J. Nemanich,

Department of Physics, North Carolina State University, Raleigh, NC 27695 USA

Abstract:

Thermionic emission and ultraviolet photoemission spectroscopy (UPS) were employed to determine the temperature dependent electron emission energy distribution from nitrogen doped diamond films prepared by microwave plasma chemical vapor deposition (CVD). The photoemission spectra obtained at room temperature indicated a work function of 1.8eV and a negative electron affinity (NEA). The thermionic emission and photoemission spectra obtained at 380°C indicated a minimum kinetic energy of 1.5eV relative to the Fermi level. Both spectra displayed the same sharp cutoff corresponding to the conduction band minimum (CBM). The temperature dependence of the Fermi energy and the surface band bending were modeled to account for the work function reduction with increased temperature.

3.1 Introduction

Vacuum thermionic emission, described by the Richardson equation [1], has widely been investigated for cathode applications for vacuum tube electronics and microwave devices. Thermionic emission can also be employed for energy conversion. A thermionic converter is a device which convert heat into electrical power directly [2]. However, the main difficulty to design such a device working at lower temperature for more applications was to achieve the lower work function materials. Diamond materials with a negative electron affinity (NEA) [3,4] have recently been considered to be a potential candidate for low work function applications because the Fermi level could be increased in the band gap by doping, while the surface termination will maintain the vacuum level below the conduction band minimum [5]. Additionally, diamond materials exhibit unique thermal, mechanical, chemical and electrical properties which may be appropriate for vacuum thermionic emission applications.

Nitrogen is a common impurity in both natural and CVD diamond. It is a deep donor in diamond with a level typically assigned at 1.7 eV [6] below the conduction band minimum which has been attributed to a Jahn-Teller distortion. Both theory and experiment have shown that nitrogen has a high solubility in diamond [7,8]. Furthermore, uniform electron emission was shown from N-doped CVD diamond films by photo electron emission microscopy (PEEM) and field electron emission microscopy (FEEM) characterization at temperature above ~600°C [9]. Additionally, recent results from our laboratory have indicated that nitrogen doped CVD diamond exhibits a reduced work function and increased performance of thermionic emission [5].

Previously, Diederich et al. [10] measured UPS of N-doped, type Ib diamond (100) surfaces at a temperature of 400°C and deduced that the surface Fermi level is located at 3.3eV below the CBM. They attributed the large work function to upward band bending at the surface. In this paper, we report the observation of thermionic emission at a temperature of less than 200°C and a much lower work function for N-doped CVD diamond films.

3.2 Experiment

Nitrogen-doped diamond films were prepared on 25 mm-diameter polished molybdenum substrates by microwave plasma-assisted chemical vapor deposition using a three-step growth method. Firstly, an initial buffer layer on Mo was synthesized using 400 sccm hydrogen and 8 sccm methane at a chamber pressure of 20 Torr, microwave power of 600 W and a substrate temperature of 660°C. Next, a nitrogen-doped poly-crystalline diamond layer was grown using 400 sccm hydrogen, 2.5 sccm methane, 60–100 sccm nitrogen, at a chamber pressure of 50 Torr, a microwave power of 1300 W and a substrate temperature of 900°C. The final step was a 1 minute hydrogen/deuterium passivation, where the temperature was lowered to 650°C, the chamber pressure dropped to 20 Torr and the microwave power reduced to 600W. During the deposition process, laser reflectance interferometry was used to monitor the thickness and growth rate of the buffer layer and doped diamond layer.

The emission properties of N-doped diamond samples were characterized with temperature dependent UV-photoemission spectroscopy and thermionic emission spectroscopy. The measurements were carried out in a UHV chamber with a base pressure of ~$3x10^{-10}$ Torr. Ultraviolet photoelectron spectra were obtained with He I (21.2eV) radiation from an Omicron HIS13 discharge lamp, and the emitted electrons

were measured with a VSW-HA50 hemispherical analyzer operating at a resolution of 0.1 eV. Thermionic emission spectra can be obtained with the same electron analyzer (without UV excitation). The temperature range of the measurements was limited to 600°C to avoid damage to the electron analyzer. The elevated sample temperature in the spectroscopy measurements was achieved by radiative heating from a tungsten coil filament mounted on a boron nitride disk behind the sample. A chromel–alumnel (K-type) thermocouple as well as optical pyrometer (MIKRON-M90Q) was employed to measure the sample surface temperature for temperatures above 250°C. Temperature measurements below 250°C were obtained by linear extrapolation of the thermocouple-pyrometer calibration curve. The electron spectrometer was calibrated using an in situ deposited gold film, and measurements were obtained under UV irradiation at temperatures up to 600°C. To discern the temperature dependent emission properties, all spectroscopy measurements were performed with both increasing and decreasing temperature cycles.

3.3 Results and Discussion

A typical UV photoemission spectrum from CVD nitrogen doped diamond with hydrogen termination is shown in Fig.3.1 The valence band maximum (VBM) and work function (Φ) can be directly determined in UPS. The electron affinity (χ) can be deduced from the photoemission spectrum using $\chi = h\nu$ - W - $E_{g,}$ where $h\nu$ is the photon energy (21.2 eV), E_g is the band gap and W is the spectral width from the VBM to the low kinetic energy cut off. The spectrum shown in Fig.3.1 exhibits a width of 16eV, thus with the 5.2eV band gap, we obtain a zero or negative electron affinity. For NEA semiconductors, the sharp peak at low kinetic electron energies represents the energy position of the conduction band minimum. The vacuum level is

below the conduction band minimum and the exact position of the vacuum level can not be determined by UPS alone. In the N-doped CVD diamond spectra shown in Fig.3.1, at 380°C, the Fermi level is determined to be 1.5eV below the conduction band minimum and the valence band maxim (VBM), determined by linear fitting, is ~3.7eV below the Fermi level. It is interesting to note that emission is detected below the sharp low kinetic energy cutoff at the CBM, This emission extends to 1.5±0.1eV below the CBM. Moreover, this emission intensity increases with increasing the temperature.

For most metals with 4~5eV work functions, thermionic emission can only be detected for temperatures above 800~1100^{o}C. At theses conditions, a small electron current (10^{-11}A/cm^{2}) will be emitted into vacuum as described by the Richardson equation $J=AT^{2}\exp(-\Phi/k_{B}T)$, where A is the Richarson constant, T is absolute temperature, Φ is the work function and k_{B} is the Boltzmann constant. In fact, thermionic emission from these N-doped diamond surfaces can be detected for temperature as low as 200^{o}C. In Fig.3.1, TES at 380°C has the same low kinetic energy cut off at 1.5eV referenced to the Fermi level as is observed in the UPS. This indicates that the thermionic electron emission originates from the conduction band of the NEA diamond. A diagram that relates the band energy of N-doped diamond and the UPS and TES is shown in Fig.3.2.

Figure 3.3 depicts the temperature dependent work function deduced from the UPS and/or TES measurements. At room temperature, UPS indicates a work function of 1.8eV. As the temperature is increased, the low energy cut off in both the UPS and TES display the same cutoff which decreased with increasing temperature. The work function of different N-doped diamond films does vary with the growth processes.

However, all samples showed the same trend, namely that with increasing temperature the work function decreases.

The temperature dependent work function observed in the N-doped diamond could be treated by semiconductor statistics [11]. Hensley [12] has noted that a temperature dependent electron affinity and Fermi energy will contribute to a work function change in nonmetallic cathodes. In this case, we only consider the Fermi energy issue because thermionic electrons are presumed emitted from the conduction band of N-doped diamond with NEA properties. It is also necessary to note that the hydrogen/deuterium surface termination is expected to passivate the carbon dangling bonds [3] and remove surface state bands that lead to the Fermi level pinning. Since N-doped diamond exhibits a deep donor level (1.7eV) and the nitrogen donors in diamond are hardly ionized, the population of electrons in the conduction band is much smaller than that at the N donor level. Under this assumption, the temperature and donor concentration dependent Fermi energy can be written as [11-13].

$$E_f - E_c = -E_D + k_B T \ln \frac{N_d - N_a}{2N_a} \qquad (N_d > N_a) \qquad (1)$$

where E_f is Fermi energy, E_C is conduction band minimum, E_D is donor level, k_B is Boltzmann's constant, T is absolute temperature, and N_d and N_a are donor and acceptor concentration respectively. Collins [13], using the same equation, stated that Fermi level in diamond, at 1.6eV below the conduction band minimum at room temperature, was slightly influenced by increasing the nitrogen incorporation. Nevertheless, the Fermi energy changes become more significant for higher nitrogen concentration and higher temperature. Fig 3.3 presents the temperature dependence of the Fermi energy for different nitrogen donor concentrations. For a diamond sample with N doping of $10^{19}/cm^3$, the change of Fermi energy is ~0.2eV as the temperature

is increased to 400°C. If the Fermi level at the surface is unpinned, the work function would be reduced by the same value. This calculation gives insight to our experimental observations that (1) with increasing the surface nitrogen doping concentration in diamond, the work function decreases and (2) with increasing the temperature, the work function decreases.

Although N-doped CVD diamond with hydrogen termination shows no detectable surface states, band bending still could occur when there are impurity and defect related surface charges. It is possible to introduce defects in the band gap or at the surface during CVD growth and hydrogen passivation. A surface state density less than $10^{11}/cm^2$ cannot pin the surface Fermi level at all temperatures [14]. By evaluating the Fermi level (E_{CBM}-E_F) of 1.8eV at the surface and 1.6eV in the bulk at room temperature, 0.2eV upward band bending of this nitrogen doped CVD diamond is estimated. we assume that the defect trap/state is nearly fully occupied and there are few electrons exchange between the defect surface states and the bulk of the diamond at our measurement temperatures. Since the Fermi-Dirac distribution is a temperature dependent function and need to be fixed value to keep constant surface electron population, the energy position of defect trap/state will move downward in the band gap (E-E_f increasing) when the temperature T is increased. Therefore, the band bending decreases at surface. When the surface electronic state is 99% filled ($f(E)=0.99$), band bending as well as the work function will change ~0.2eV at 400°C compared with room temperature and nearly flat band are expected. The band bending reduction could play a significant role to enhance the thermionic emission from NEA N-doped diamond because it lowers the surface barrier for electron transport to the surface and enhances the vacuum thermionic emission.

The electron emission below the CBM of NEA diamond had been detected previously and used for vacuum level determination. Experimental investigations by Baumann et al. [15] suggested that extended hydrogen or deuterium plasma treatment on diamond surface could strongly influence the emission below the CBM. However, the mechanism of the electron emission below CBM is still controversial. Bandis et al. [16] attributed this feature to the exciton breakup mechanism. Yater et al. [17] proposed that the below CBM electron emission could occur if electrons lose energy under situations of inelastic scattering at the surface/vacuum interface or transitions to low-energy surface states. Ristein et al. [18] attributed it to the defect emission under thermal non-equilibrium. Despite the undetermined origin of the emission below the CBM, from Fig.3.1, it is interesting to note that the vacuum level is near the diamond Fermi level with specifying the vacuum level position with the onset of electron emission. By the definition of semiconductor work function as the energy difference of vacuum level referenced to the Fermi level [4,19], our results indicate zero or negative true work function of N-doped CVD diamond. The barrier to the thermionic emission in this case is then the energy to the CBM and not the vacuum level.

3.4 Conclusions

Combined UPS and TES measurements have established that thermionic electrons are emitted from the conduction band minimum of N-doped diamond at temperatures above 200°C. The measurements showed that the work function decreased as the temperature was increased. The temperature dependent work function of the N-doped diamond was ascribed to contributions from Fermi energy and surface band bending effect. This low work function N-doped CVD diamond films have indicated potential suitability for vacuum thermionic energy conversion.

Acknowledgement

This work is supported by the Office of Naval Research (ONR) under the Thermionic Energy Conversion (TEC) - Multidisciplinary University Research Initiative (MURI) project.

3.5 References:

[1] C. Herring and M. H. Nichols, Rev. Mod. Phys. **21**, 185 (1949).

[2] N. S. Rasor, J. Appl. Phys. **31**, 163 (1960).

[3] J. Vanderweide, Z. Zhang, P. K. Baumann, M. G. Wensell, J. Bernholc, and R. J. Nemanich, Phys. Rev. B **50**, 5803 (1994).

[4] J. B. Cui, J. Ristein, and L. Ley, Phys. Rev. Lett. **81**, 429 (1998).

[5] F. A. M. Koeck and R. J. Nemanich, Diam. Relat. Mat. **15**, 217 (2006).

[6] R. G. Farrer, Solid State Commun. **7**, 685 (1969).

[7] S. A. Kajihara, A. Antonelli, J. Bernholc, and R. Car, Phys. Rev. Lett. **66**, 2010 (1991).

[8] S. Jin and T. D. Moustakas, Appl. Phys. Lett. **65**, 403 (1994).

[9] F. A. M. Kock, J. M. Garguilo, and R. J. Nemanich, Diam. Relat. Mat. **10**, 1714 (2001).

[10] L. Diederich, O. Kuttel, P. Aebi, and L. Schlapbach, Surf. Sci. **418**, 219 (1998).

[11] J. S. Blakemore, *Semiconductor Statistics* (Dover Pubns, New York, 1987).

[12] E. B. Hensley, J. Appl. Phys. **32**, 301 (1961).

[13] A. T. Collins, J. Phys.-Condes. Matter **14**, 3743 (2002).

[14] H. Lüth, *Interfaces and Thin Films* (Springer, Berlin, 2001).

[15] P. K. Baumann and R. J. Nemanich, Surf. Sci. **409**, 320 (1998).

[16] C. Bandis and B. B. Pate, Phys. Rev. B **52**, 12056 (1995).

[17] J. E. Yater, A. Shih, and R. Abrams, Phys. Rev. B **56**, R4410 (1997).

[18] J. Ristein, W. Stein, and L. Ley, Phys. Rev. Lett. **78**, 1803 (1997).

[19] M. Cardona and L. Ley, *Photoemission in Solids I* (Springer, Berlin, 1978).

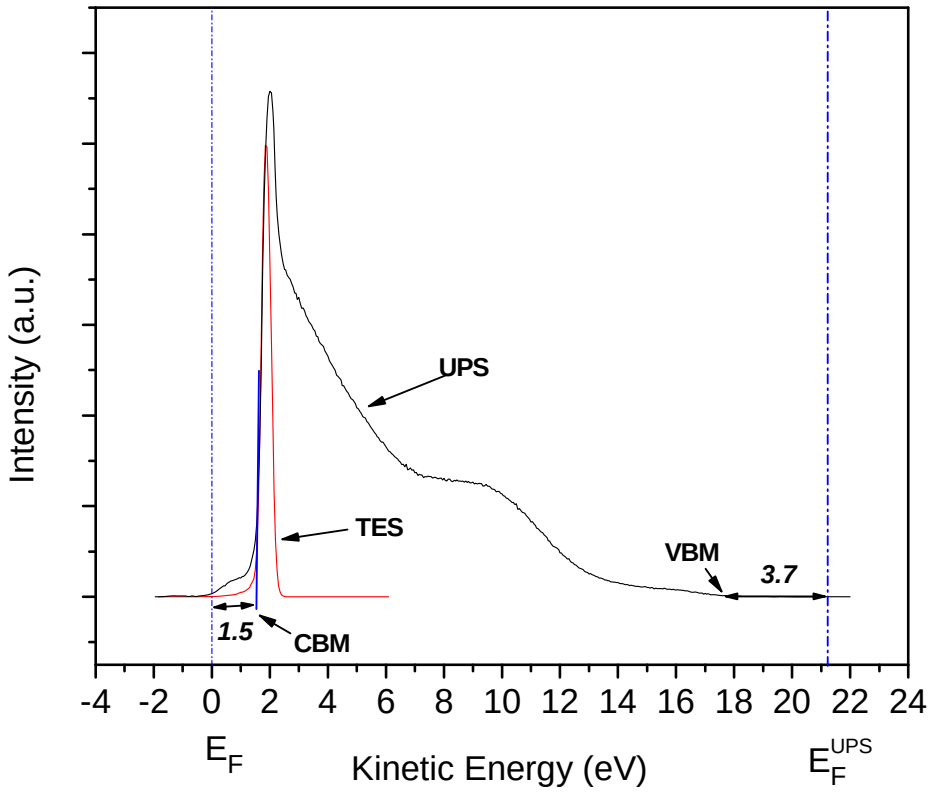

Figure 3.1 Electron emission from N-doped CVD diamond at 380°C: UV photoemission spectrum (upper) and thermionic emission spectrum (lower). The 0 of the spectrum is located at the Fermi level (E_F) of the sample and the E_F^{UPS} is 21.2 eV above the Fermi level.

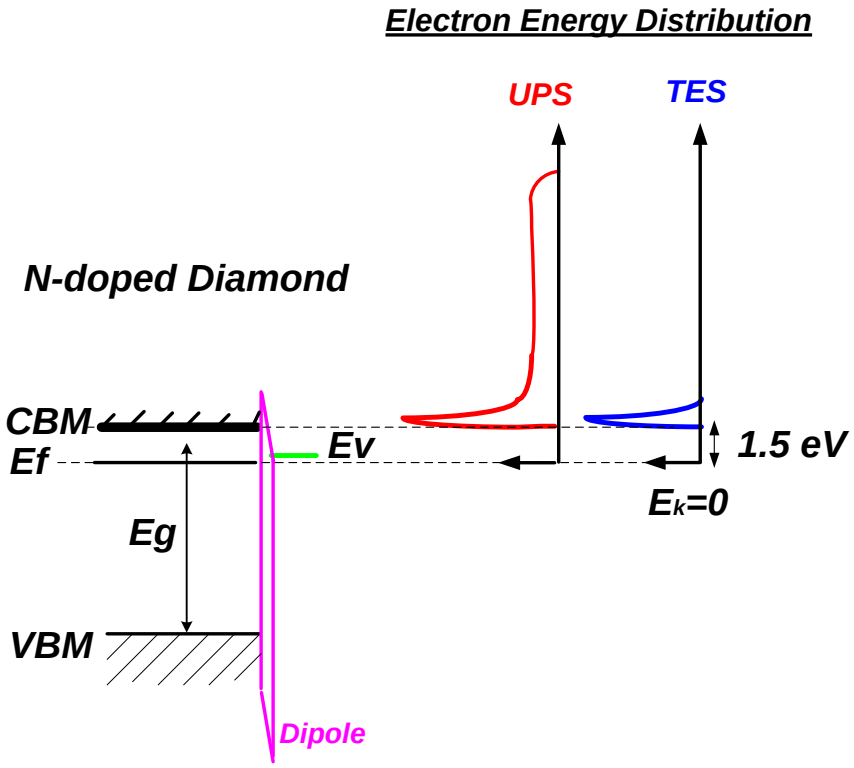

Figure 3.2 Band schematic and the UPS and TES spectra that would be obtained from a low work function diamond sample. In the schematic, the vacuum level is reduced below the CBM by the surface dipole from the chemisorbed hydrogen.

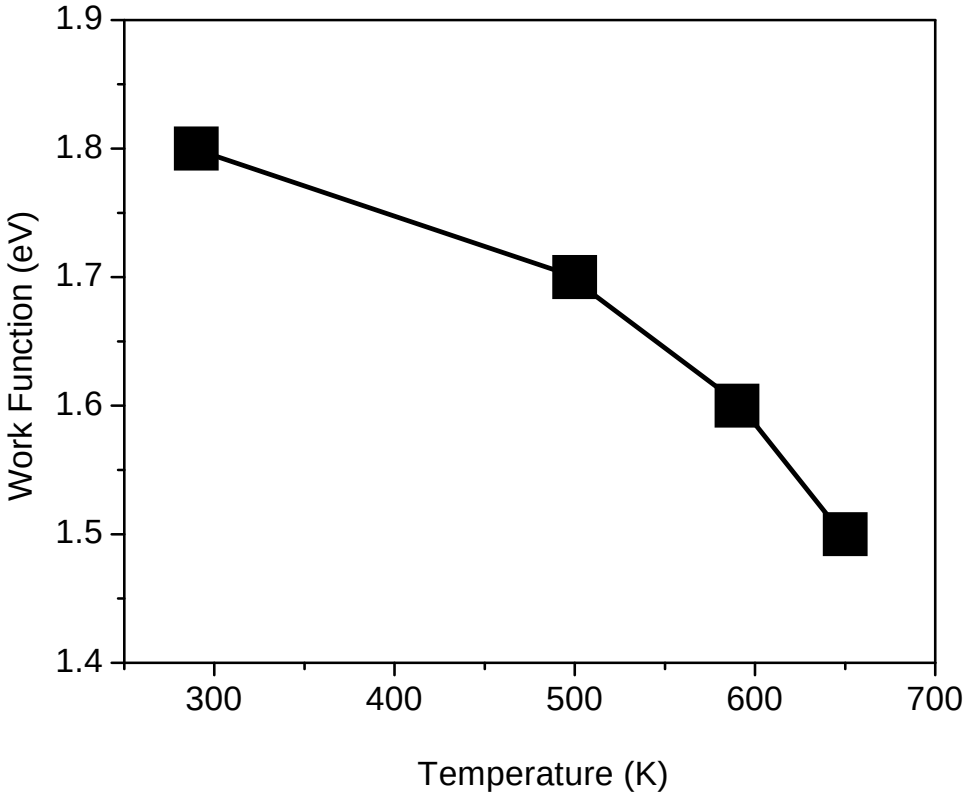

Figure 3.3 Temperature dependent work function of the N-doped CVD diamond film derived from the UPS and TES measurements.

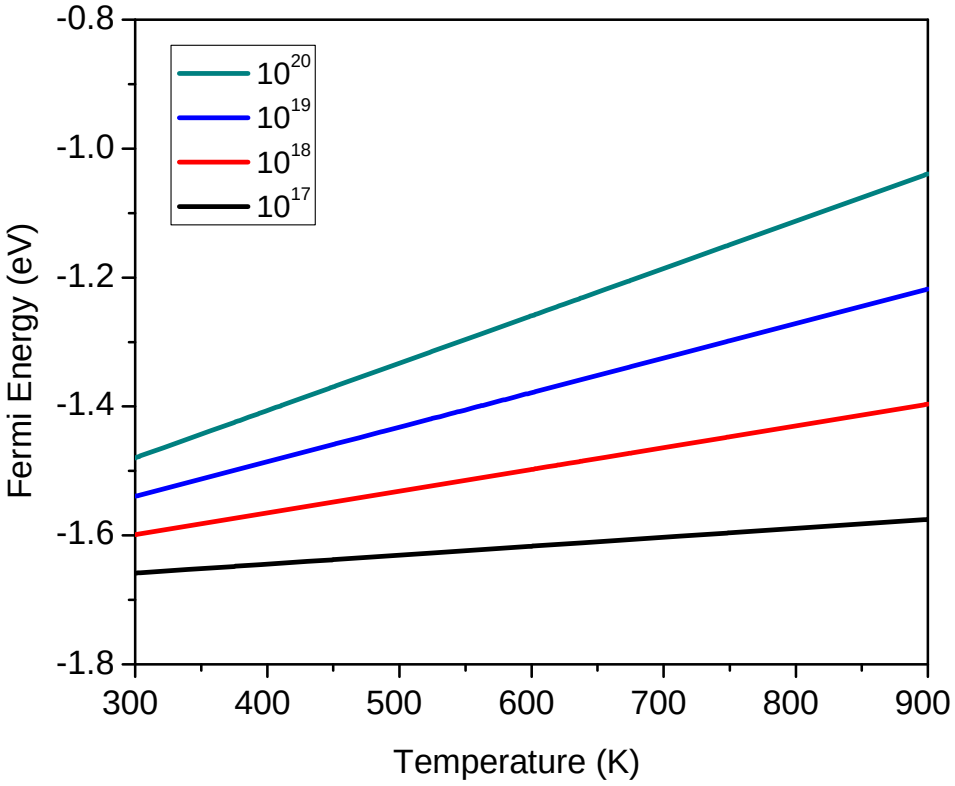

Figure 3.4 A calculation of temperature and nitrogen donor concentration dependent Fermi energy in diamond assuming a donor level at 1.7 eV below the conduction band minimum.

4. Properties of Nitrogen Doped CVD Diamond for Thermionic Emission

Yingjie Tang, Franz A. M. Koeck and Robert J. Nemanich,

Department of Physics, North Carolina State University, Raleigh, NC 27695 USA

Abstract:

Nitrogen doped CVD diamond films were investigated by X-ray photoemission spectroscopy (XPS), ultraviolet photoemission spectroscopy (UPS) and thermionic emission spectroscopy (TES) to determine the relationship of the electron emission processes and the surface electronic properties. Thermionic emission was observed at a temperature of 380ºC where the emission cut on was at 1.5 eV above Fermi level which corresponded to emission from the conduction band minimum. The increased binding energy of the VBM (3.7eV) and the C1s core level (286.6eV) were indications of the increase of the Fermi level within the bandgap. The difference of surface band bending for the CVD diamond in comparison with results for natural single diamond was discussed regarding the donor and acceptor surface state. A band diagram was proposed to describe the electron transport and thermionic emission process for the N-doped diamond thin film structure. The coupling of the sp^2 and sp^3 bonded carbon appears to play an important role in the electron transport.

4.1 Introduction

One of the key issues in the development of thermionic emission sources is obtaining a low work function material.[1] Diamond and related materials which exhibit a negative electron affinity[2] have been considered as potential candidate low work function materials because the Fermi level could be increased in the band gap by doping, while the surface termination will maintain the vacuum level below or near the conduction band minimum. Additionally, diamond materials exhibit unique thermal, mechanical, chemical and electrical properties and are suitable for the vacuum thermionic emission applications. These materials could be used in a thermionic energy converter which can efficiently convert heat to electrical energy and which would operate at temperatures less than 1000K.

A surface exhibits negative electron affinity (NEA) when the conduction band minimum energy lies above the vacuum energy level. The electrons at the conduction band can then escape into vacuum without passing an energy barrier. Research has established that ultraviolet photoemission spectroscopy (UPS) can be used to determine the electron affinity of a semiconductor from the measured width of the spectrum and the presence of the characteristic sharp peak at the low-energy tail of the photoemission spectrum. due to the emission of secondary electrons accumulated at the conduction band minimum.

CVD diamond films can be prepared with a high concentration of nitrogen, and studies of crystalline diamond have established that the material exhibits a deep donor level located 1.7 eV below the conduction band minimum.[3] Recently, it has been reported that N-doped CVD diamond films show low work function properties,[4] and they display uniform thermionic emission at temperatures noticeably less than 800ºC.[5]

Previously, most emission studies of thermionic emission involved a curve fitting analysis of the current–temperature data using the Richardson equation. While the work function is predicted to be the only materials dependent parameter, it is found that the Richardson constant also varies significantly for different materials. Thus the emission current vs temperature is dependent on both the work function and the Richardson constant and it is often difficult or impossible to determine unique values from fitting the experimental data.

An alternative approach involves deducing the work function from the spectrum of the thermionic emission. This approach provides a unique value of the work function. For example, Robinson et al.[6] deduced a work function 2.2eV for potassium intercalated graphitic nanofibers based on an analysis of the spectrum of the thermionic emission at 600^{o}C.

Since the diamond materials are semiconducting the thermionic emission spectrum is insufficient to completely characterize the emission. In this study, both photoemission and thermionic emission are employed to develop a complete characterization of the properties of the surface related to thermionic emission. The photoemission spectrum is employed to determine the electron affinity, and the thermionic emission spectrum is employed to deduce the work function. The results can also be employed to deduce the band bending at the surface. This spectroscopic approach using thermionic and photo-emission provides the essential characterization to develop an understand of the physical emission process from negative electron affinity (NEA) emitters.

4.2 Experiment:

Nitrogen-doped diamond films were synthesized utilizing plasma-assisted chemical vapor deposition. The films were deposited on 1-in. diameter polished molybdenum disks to obtain a low electrical resistance for the structure. To enhance the nucleation, the films were sonicated in a solution containing diamond particles and titanium particles and thoroughly rinsed to remove any large particles. The initial buffer layer with a high sp^2 density was synthesized using 400 sccm hydrogen and 8 sccm methane at a chamber pressure of 20 Torr, microwave power of 600 W and a substrate temperature of 660°C. Next, a nitrogen-doped poly-crystalline diamond layer was grown using 400 sccm hydrogen, 2.5 sccm methane, 60–100 sccm nitrogen, at a chamber pressure of 50 Torr, a microwave power of 1300 W and a substrate temperature of 900°C. The final step was a 1-minute hydrogen/deuterium passivation, where the temperature was lowered to 650°C; the chamber pressure dropped to 20 Torr and the microwave power reduced to 600W. The film growth for each grow step was monitored by in situ laser interferometry. Over 20 nitrogen-doped CVD diamond samples were grown under similar process conditions and studied.

X-ray photoemission spectroscopy (XPS) were performed in UHV with a base pressure of $2x10^{-10}$ Torr, using a dual anode Mg/Al x-ray source and a 100 mm diameter hemispherical electron energy analyzer VG CLAM II. The settings for the x-ray source were 5 A filament current, 20 mA emission current, 13 kV accelerating voltage. The analyzed channeltron was set at 3.0 kV, and survey scans and core level spectra were collected using pass energies of 50 and 20 eV, respectively. Calibration of the binding energy scale was achieved by measuring the Au $4f_{7/2}$ peak of a freshly deposited film. A Gaussian–Lorentzian peak function was employed with a linear

background subtraction, and the curve fitting could determine the peak positions with a precision of ±0.1 eV.

The ultraviolet photoemission spectra (UPS) were obtained with He I (21.2eV) radiation from an Omicron HIS13 discharge lamp and a VSW-HA50 hemispherical analyzer. The lamp voltage and discharge current were set to 520 V and 50 mA, respectively. The resolution of the 50 mm mean radius hemispheric analyzer was approximately 0.1 eV. Thermionic emission spectra (TES) could be obtained with the same electron analyzer but the UV light off. The elevated sample temperature in the spectroscopy measurements was achieved by radiative heating from a tungsten coil filament mounted on a boron nitride disk behind the sample. A chromel–alumnel (K-type) thermocouple and an optical pyrometer (MIKRON-M90Q) were employed to measure the sample surface temperature for temperatures above 250°C. Temperature measurements below 250°C were obtained by linear extrapolation of the thermocouple-pyrometer calibration curve.

Room temperature Raman spectra were recorded with an ISA U-1000 scanning double monochromator using the 514.5 nm line of an argon ion laser as the excitation source. Scanning electron microscopy (SEM) images were obtained with an JEOL 6400 using a beam energy of 5 kV.

4.3 Results and discussion

4.3.1 XPS, UPS and TES

An XPS spectrum of the nitrogen doped diamond film used in this study is shown in Figure 4.1. The XPS analysis indicated that the oxygen peak signal around

532.0eV was below the detection limit of the samples with hydrogen termination. and after peak fitting the C 1s core level was found at 286.6 eV. However, McFeely[7] showed diamond have C 1s core level binding energies at 284.44 eV. It is assumed the spacing between a core level and the valence band maximum to be constant and using Fermi level as a reference in XPS. The higher C 1s binding energy than previously reported values of carbon in diamond is attributed to the Fermi level position in the nitrogen doped film. For n-type doping the Fermi level will occur in the upper half of the gap and will increase the binding energy of all levels by the same amount. The increased nitrogen doping is not incorporated into diamond films to the amount detectable by XPS.

Figure 4.2 shows a temperature dependent UV photoemission spectra of N-doped CVD diamond film with hydrogen termination as a function of temperature. The UPS spectra were measured while the sample was biased by negative 4 V to overcome the analyzer work function and to eliminate artifacts of the electron analyzer. The electron affinity of a semiconductor could be determined from the photoemission spectrum using the realtion $\chi = h\nu$ - W - $E_{g,}$ where $h\nu$ is the photon energy (21.2 eV), E_g (5.4eV) is the band gap and W (16.0±0.1eV) is the spectral width from the valence band maxim (VBM) to the low kinetic energy cut off. According to this analysis the electron affinity of the surface is -0.2±0.1. We note that UPS can not be used to determine the value of a surface with a negative electron affinity, but previous results have indicated that for H-terminated diamond the vacuum level is at 1.2 eV below the CBM[8]. The effective work function of an NEA emitter is the energy difference between the Fermi level and the conduction band. All of the spectra have been analyzed using the same approach. It is found that the work

function decreases from 1.8eV at room temperature to the 1.5eV as the temperature is increased to 380^{o}C.

We call attention to an unusual aspect of the photoemission spectrum. Emission is observed in the region below the conduction band minimum and above the Fermi level. This emission probably originates from a combination of surfaces states and sp^2 bonded carbon near or at the surface indicates. The emission also suggests that the vacuum level is within a few tenths of an eV of the Fermi level.

TES measurements were performed to determine the origin of the thermionic emitted electrons in the nitrogen doped diamond films. We presume that the integrated count rate would be proportional to the thermionic emission current. Figure 4.3 illustrates the temperature effect on the thermionic emission. At 200^{o}C, thermionic emission was observed by TES with cut off at 1.7eV, corresponding to an effective work function of approximately 1.7 eV. These results are in agreement with the work function that was deduced from the UPS results. The bias dependent thermionic emission spectroscopy shows that the spectra shift by the same value as the applied bias. The peak cut off appears to correspond to the CBM and the peak shape does not significantly change with applied negative bias. It is expected that the high-energy side of the spectrum is determined by the temperature dependent Fermi-Dirac distribution, while the low-energy cutoff side stands for of the solid-vacuum interface.

4.3.2 Composition and transport properties

The Raman spectrum of the same N-doped CVD diamond film is depicted in Fig. 4.4. The Raman spectrum displays the diamond characteristic broadening peak at about 1333 cm^{-1} which is typically assigned as the triply degenerate phonon of F_{2g}

symmetry[9, 10]. The intense background indicates significant amounts of non-diamond material. The broad feature from ~1100 to ~1600 cm^{-1} is attributed to disordered sp^2 carbon and nitrogen impurities.[10] This raman spectrum is the combination result from the top layer diamond which was confirmed by the UPS and the carbon layer including both sp^2 and sp^3 composition.

Fig. 4.5 shows a cross section SEM of the N-dope diamond film. The approximate locations of the predominantly sp^2 buffer layer and sp^3 top layer could be identified, consistent with our growth procedure. This sp^2 containing buffer layer was experimentally found to be important for the thermionic emission properties.

A proposed schematic band diagram is shown in Fig. 4.6 for the electron transport for thermionic emission from N-doped diamond grown on Mo. The emission process includes contributions from carrier injection at the back interface, conduction through the bulk, and finally thermionic emission from the surface into vacuum. The relatively thick sp^2 nucleation layer helps to keep layer intact during the growth of the heavily N-doped layer. At high N-gas phase concentrations the sp^2 bonded regions are preferentially etched. The properties of the interface between the Mo substrate and the diamond appears to be crucial for a low Schottky barrier height and efficient electron transport. The predominantly sp^2 buffer layer coupled with the sp^3 carbon bonding is expected to reduce the energy barrier at the substrate and increase the conductivity for the electrons injected from the Mo into the conduction band of diamond.

This structure effectively represents band gap engineering which is controlled by the relative sp^2 and sp^3 fractions in the layers and the nitrogen doping which increases the Fermi energy in the doped diamond surface region of the structure. We expect that there is no significant field penetration into the diamond layer because the

several volt bias is over the 3cm distance between the sample and the grounded analyzer is so small the effect will be negligable.

The H processing is necessary for thermionic emission. If the sample is heated to the extent that the hydrogen evolves from the surface, the thermionic emission is no longer detectable. It is anticipated that the H termination serves to induce an NEA and to passivate dangling bonds and surface states. It is interesting that these surfaces do not show the strong upward band bending that has been reported in N-doped crystalline diamond surfaces. This is discussed in the next section.

4.3.3 Comparison with N-doped single crystal diamond

Fig 4.7 (a) displays a UV photoemission spectrum of N-doped single crystal diamond obtained at 600°C. We were unable to make the measurements at lower temperature due to charging of the sample surface during the photoemission process. The results indicate the valence band maximum is 2.0 eV below the Fermi level and a zero or negative electron affinity was determined due the spectra width of 15.8eV. This value of W is different from the 16.0 value used in Fig 4.2. The heavily doped nitrogen and sp2 impurities in CVD diamond could have the band tail effect to reduce the energy gap value. The low kinetic energy cut off is 3.4eV above the material Fermi level, which is similar to the 3.3 eV result reported by Diederich et al.[11, 12]. The band diagram derived from the UPS is shown in Fig 4.7 (b). The 1.7 eV deep level [3] of the single substitutional nitrogen donor in diamond has been attributed to a Jahn-Teller distortion. Using semiconductor statistics, the Fermi level in the bulk can be derived from the equation[13, 14]

$$E_f - E_c = -E_D + k_B T \ln \frac{N_d - N_a}{2N_a}$$

where E_f is Fermi energy, E_C is conduction band minimum, E_D is donor level, k_B is Boltzmann's constant, T is absolute temperature, and N_d and N_a are donor and acceptor concentration respectively. At 600°C this expression yields a Fermi level at 1.2 eV below the conduction band. The surface band bending in the N-doped single crystal diamond was 2.2eV. This large band bending was also account for the non-sharp low cut-off peak at conduction band as observed Fig 4.7 (a).

Band bending could occur when there are impurity and defect related surface charges[15]. It is considered that the hydrogen/deuterium surface termination is expected to passivate the carbon dangling bonds[2] and remove the π-bonded surface state bands that lead to the Fermi level pinning. However, σ-bonded surface states are almost unaffected[16]. The introduction of nitrogen donors could populate the unoccupied surface states but this does not appear to be sufficient for the single crystal surface, and a large upward band bending is always observed. In contrast, the N-doped CVD diamond films only showed negligible 0.1-0.2eV band bending. It seems then that the presence of the sp^2 bonded regions in the film tends to compensate or eliminate the surface states responsible for the upward band bending. Moreover, it has been reported that nitrogen incorporation leads to significant changes in the relative amount of sp^2-bonded carbon[17].

4.4 Conclusion

The use of XPS, UPS and TES for the study of thermionic emission properties of nitrogen doped diamond films provides insight into the mechanisms of low temperature emission in diamond thermionic cathodes. Using UPS, NEA characteristics were detected on the surface of N-doped diamond deposited on layered structures. From the TES and UPS it was established that the thermionic electrons

originate from the conduction-band minimum at 1.5 eV above the Fermi level at 380^{o}C. The increased binding energy of the VBM (3.7eV) and C1s (286.6eV) core level were considered as evidence of the movement of the Fermi level towards the upper region of the bandgap.

A band diagram was proposed for electron transport through the substrate interface and including thermionic emission from the N-doped diamond surface layer. It was proposed that sp^2 and sp^3 bonds and coupling plays an important role in reducing the energy barrier. The difference of the surface band bending at the CVD diamond and single crystal diamond surfaces was discussed in relation to the development of or compensation of surface states.

This work is supported by the Office of Naval Research (ONR) under the Thermionic Energy Conversion (TEC) - Multidisciplinary University Research Initiative (MURI) project.

4.5 References:

[1] C. Herring and M. H. Nichols, Rev. Mod. Phys. **21**, 185 (1949).

[2] J. Vanderweide, Z. Zhang, P. K. Baumann, M. G. Wensell, J. Bernholc, and R. J. Nemanich, Phys. Rev. B **50**, 5803 (1994).

[3] R. G. Farrer, Solid State Commun. **7**, 685 (1969).

[4] Y. Tang, F. A. M. Koeck, and R. J. Nemanich, unpublished.

[5] F. A. M. Koeck, J. M. Garguilo, and R. J. Nemanich, Diam. Relat. Mat. **10**, 1714 (2001).

[6] V. S. Robinson, T. S. Fisher, J. A. Michel, and C. M. Lukehart, Appl. Phys. Lett. **87** (2005).

[7] F. R. McFeely, Kowalczy.Sp, L. Ley, R. G. Cavell, R. A. Pollak, and D. A. Shirley, Phys. Rev. B **9**, 5268 (1974).

[8] J. B. Cui, J. Ristein, and L. Ley, Phys. Rev. Lett. **81**, 429 (1998).

[9] R. J. Nemanich, Annu. Rev. Mater. Sci. **21**, 535 (1991).

[10] R. J. Nemanich, J. T. Glass, G. Lucovsky, and R. E. Shroder, J. Vac. Sci. Technol. A-Vac. Surf. Films **6**, 1783 (1988).

[11] L. Diederich, O. M. Kuttel, P. Ruffieux, T. Pillo, P. Aebi, and L. Schlapbach, Surf. Sci. **417**, 41 (1998).

[12] L. Diederich, O. Kuttel, P. Aebi, and L. Schlapbach, Surf. Sci. **418**, 219 (1998).

[13] J. S. Blakemore, *Semiconductor Statistics*, 1987).

[14] A. T. Collins, J. Phys.-Condes. Matter **14**, 3743 (2002).

[15] H. Lüth, *Interfaces and Thin Films. 3rd* (Springer, 2001).

[16] J. Furthmuller, J. Hafner, and G. Kresse, Phys. Rev. B **53**, 7334 (1996).

[17] B. R. Stoner, B. E. Williams, S. D. Wolter, K. Nishimura, and J. T. Glass, J. Mater. Res. **7**, 257 (1992).

[18] J. Mort, M. A. Machonkin, and K. Okumura, Appl. Phys. Lett. **59**, 3148 (1991).

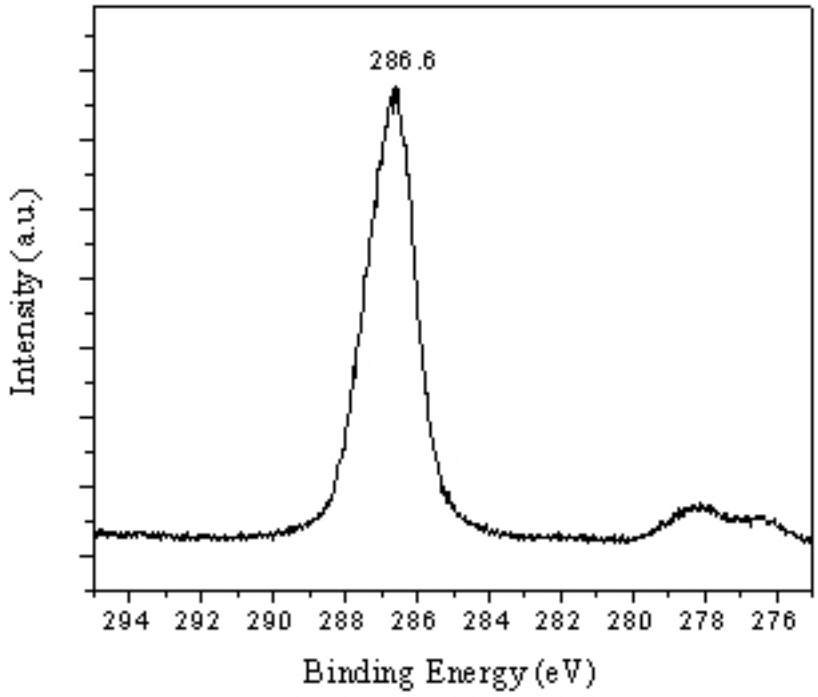

Figure 4.1 XPS spectrum of the nitrogen doped diamond film indicate the C 1s core level binding energy of 286.6 eV

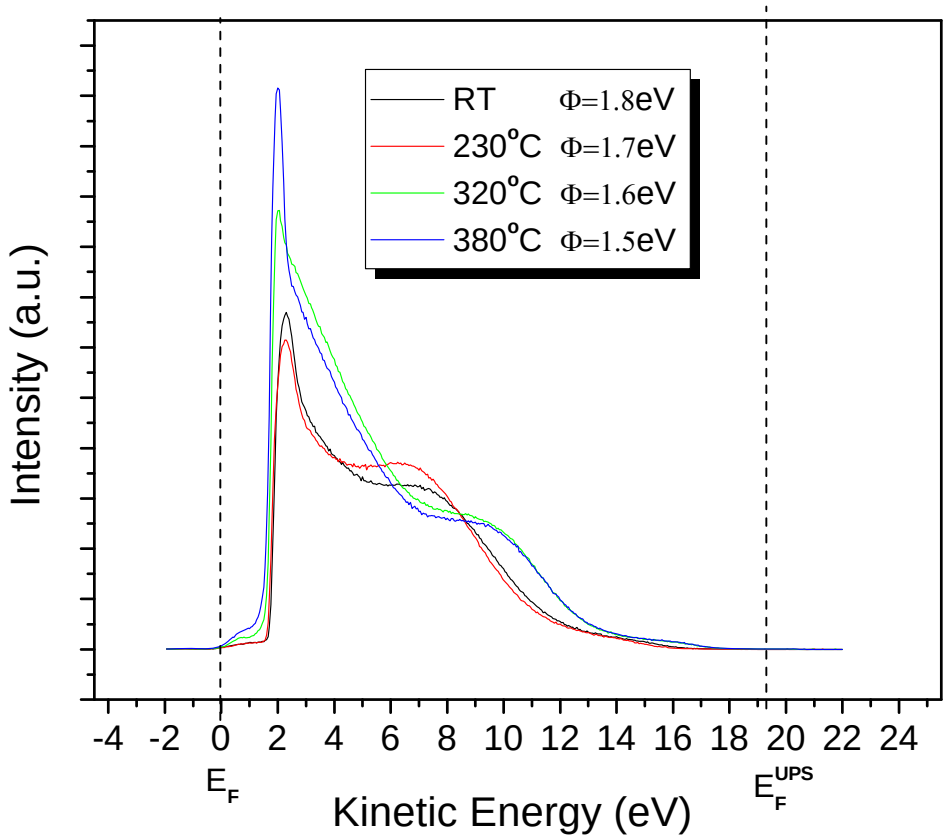

Figure 4.2 UV photoemission of N-doped CVD diamond with hydrogen termination as a function of temperature.

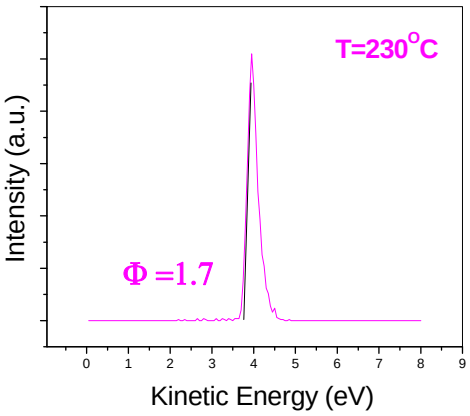

(a)

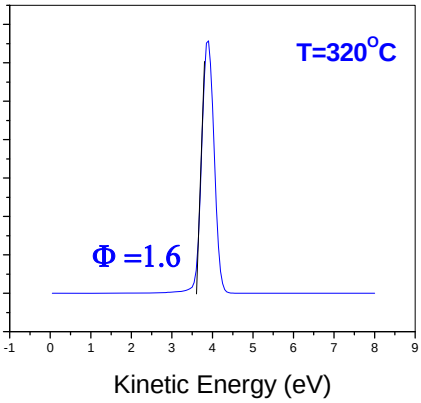

(b)

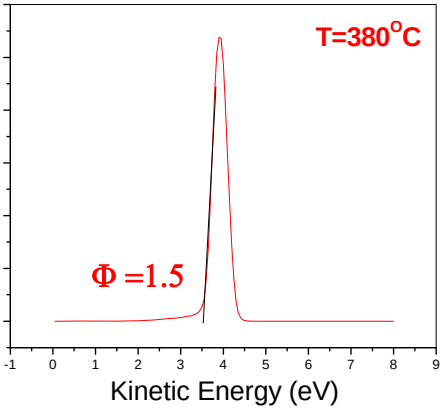

(c)

Figure 4.3 Temperature effect on the thermionic emission, corresponding to an effective work function of approximately (a) 1.7 eV at 230°C; (b) 1.6 eV at 320°C ; (c) 1.5 eV at 380°C.

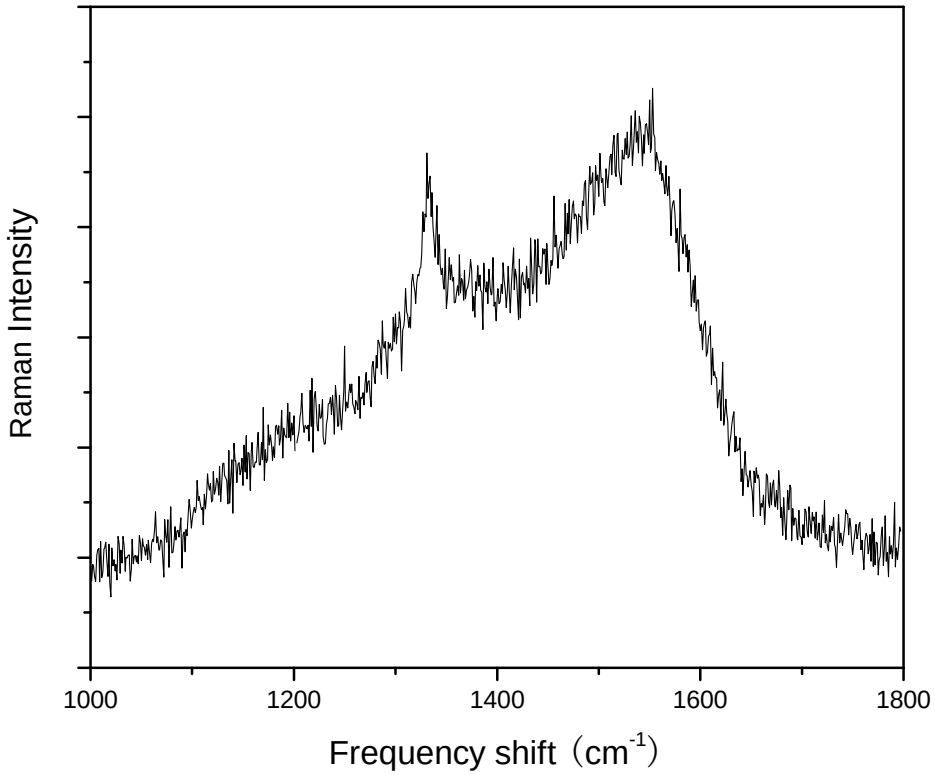

Figure 4.4 Raman spectra of N-doped CVD diamond films with diamond characteristic peak and broad sp2 related feature.

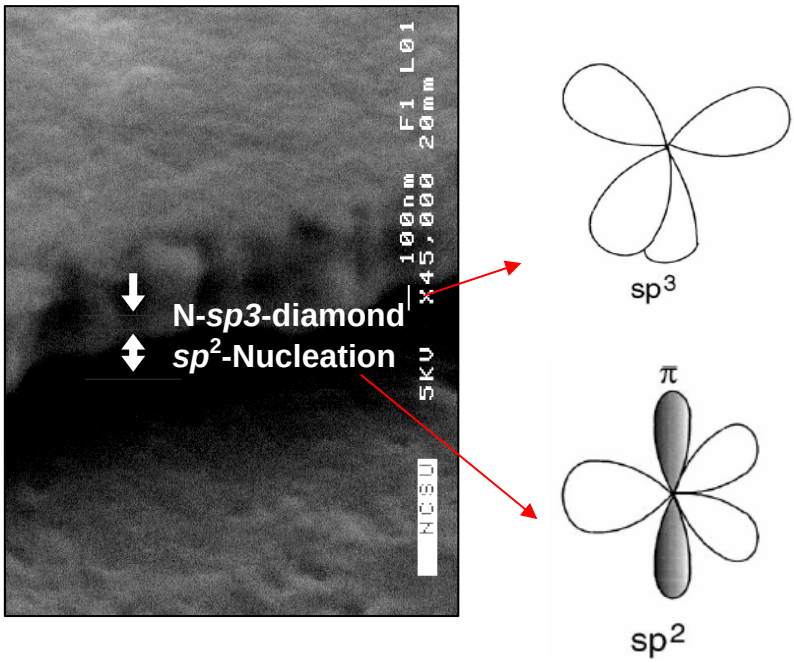

Figure 4.5 SEM of the cross section N-dope diamond describes the sp^2 and sp^3 multilayer structure.

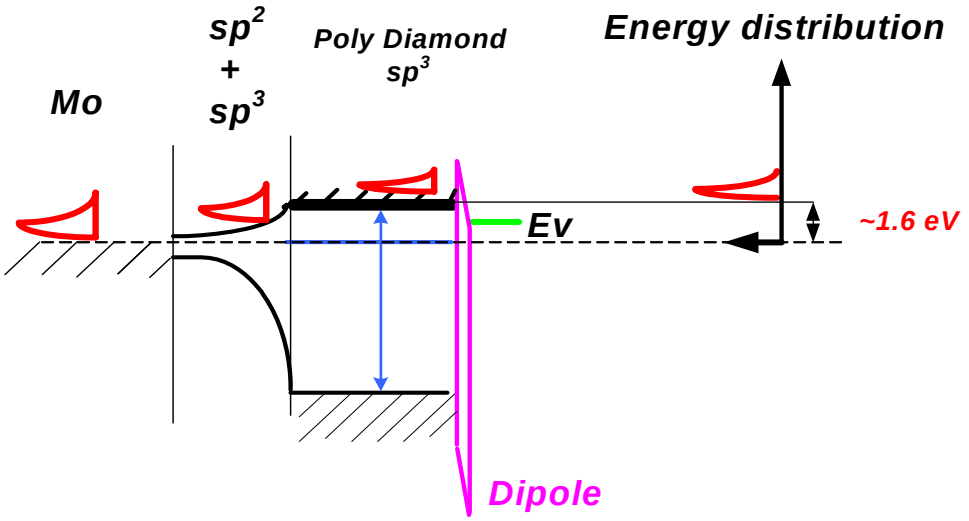

(a)

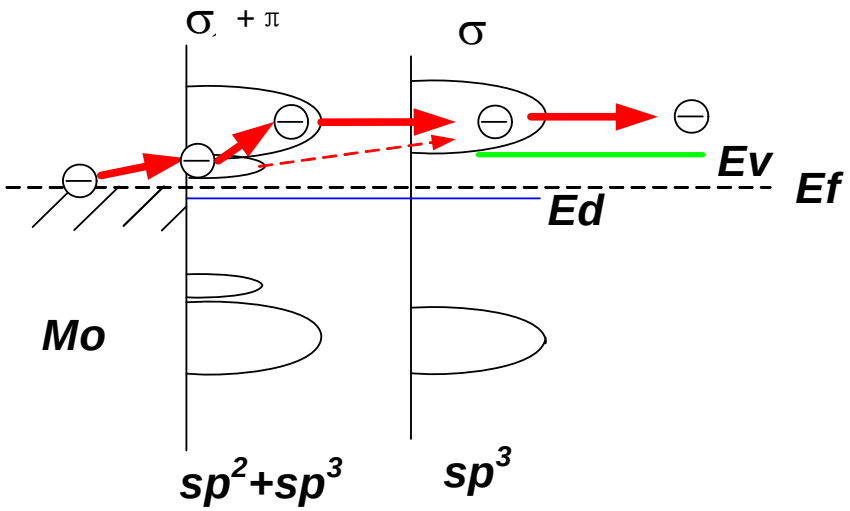

(b)

Figure 4.6 The band diagram of the electron transport for the thermionic emission from N-doped diamond grown on Mo (a) energy gap engineering (b) σ and π bonding mixture

.

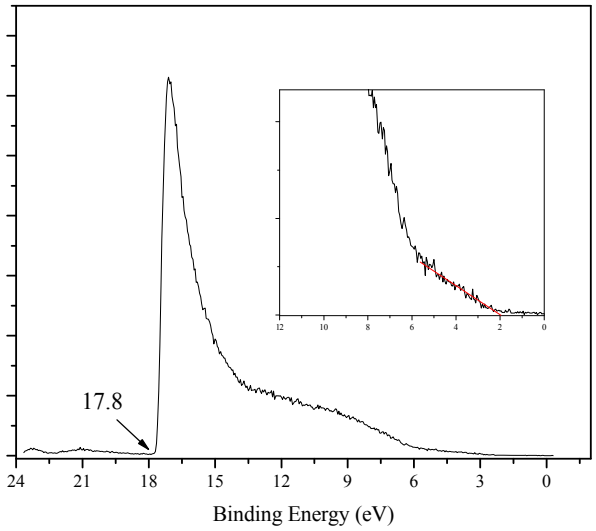

(a)

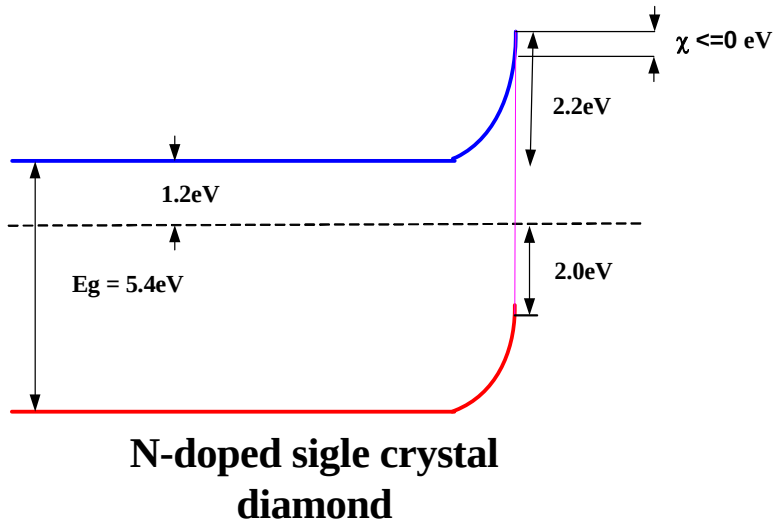

(b)

Figure 4.7 (a) showed UV photoemission spectroscopy of N-doped single crystal diamond at 600^{o}C; (b) band diagram.

5. The Effect of a Negative Electron Affinity on Thermionic Emission from N-doped Diamond

Yingjie Tang, Franz A. M. Koeck and Robert J. Nemanich,

Department of Physics, North Carolina State University, Raleigh, NC 27695 USA

ABSTRACT

The thermionic emission properties of both Dysprosium and N-doped CVD diamond with a negative electron affinity (NEA) were investigated with thermionic emission spectroscopy (TES). At a temperature of 370^{o}C thermionic emission from N-doped diamond was observed with a minimum kinetic energy of 2.5eV relative to the Fermi level, while thermionic emission from Dy was detected until temperature above 560^{O}C with 2.5eV work Function. The different thermionic emission properties between N-doped diamond and Dy were attributed to the negative electron affinity (NEA) on diamond surface. Fitting results showed thermionic emission from Dy follows the traditional Maxwell-Boltzmann distribution while the thermionic emission CVD diamond is more close to the half-Maxwellian distribution.

5.1 Introduction

Semiconductors with an effective negative electron affinity (NEA) are widely used as the photocathode for photodetectors. In these applications the effective NEA is obtained through a combination of band bending and a low electron affinity[1]. In contrast, an n-type semiconductor with a negative electron affinity could serve as an intense electron source enabled by either thermionic emission or field emission. These sources have been proposed for applications that include flat panel displays, cathodes for high frequency amplifiers, and thermionic energy conversion[2-4]. A negative electron affinity (NEA) occurs when the conduction band minimum energy lies above the vacuum energy level. An electron in the semiconductor conduction band can escape into vacuum without being impeded by an energy barrier at the surface.

An aspect of the emission that has not been considered is that the emitted electrons would have a kinetic energy equal to or greater than the value of the NEA, and this kinetic energy could influence the characteristics of a thermionic cathode.

The maximum current that can be supplied by a metallic thermionic cathode is given by the Richardson-Dushmann equation: [5] $J(T)=AT^2\exp(-\Phi/k_BT)$, where the emission current density J is dependent on the metal work function Φ, the Richardson constant A, the temperature T and the Boltzmann constant k_B. For most applications the current is limited by the negative space charge that develops just outside the surface of the cathode. In this case the emission follows the Child-Langmuir expression given by $J = A\frac{(V_B)^{\frac{3}{2}}}{d^2}$, where A is the constant, V_B is the bias and d is distance between the anode and cathode

Hydrogen terminated single crystal diamond surfaces have been shown to exhibit a negative electron affinity with a value of ~1.2 eV. Moreover, n-type character has been achieved through doping with nitrogen. Nitrogen doped natural crystals have been shown to have a deep donor level at 1.7 eV below the conduction band minimum. While this level is too deep to be effective for room temperature electronics, these donors may be activated at elevated temperatures and could contribute to a thermionic emission current. Photoemission studies of H-terminated N-doped natural single crystals indicated NEA characteristics, but strong upward band bending was detected. This upward band bending, which was presumably due to surface states, significantly increased the barrier to thermionic emission.

For a metal surface the barrier to emission is typically described as the work function, but for a semiconductor with a NEA, it is more appropriate to describe the barrier to emission as the energy from the Fermi level to the conduction band minimum.

For a semiconductor To achieve thermionic emission at moderate temperatures it is necessary to reduce the barrier to emission Diamond surfaces have been shown to exhibit a Nitrogen doped CVD diamond with hydrogen termination grown on Mo substrates had been investigated as a material for thermionic electron emitter [6] and uniform electron emission was shown by photo electron emission microscopy (PEEM) and field electron emission microscopy (FEEM) at temperature above ~600°C[7]. Nitrogen has a high solubility[8] in diamonds and deep donor level located ~1.7 eV[9] below the conduction band minimum.

This phenomenon has potential for application in electron emission devices. NEA could be easily detected by a characteristic sharp peak in the low-energy tail of

photoelectron spectra[10] that is due to the emission of secondary electrons accumulated in the conduction band minimum.

In this study we focus on the effect of the NEA on the thermionic emission from N-doped diamond films. The energy spectrum of the emitted electrons is compared to that obtained from a metal surface with a similar value of the barrier to emission. The focus of this study is to determine whether the NEA will affect the emission current and the emission spectrum.

To achieve thermionic emission at relatively low temperature we have prepared a multi-layered diamond film structure that includes a N-doped diamond film with hydrogen termination. The films contain a significant fraction of sp^2 bonded carbon which apparently contributes to a reduced band bending in comparison to the N-doped natural crystal samples.

In this article, we compared the thermionic emissions of a metallic dysprosium film with a work function of 2.4 eV with a multilayered N-doped diamond film with a similar 2.4eV barrier to emission. The thermionic emission spectra of both samples is compared to elucidate the effect of the NEA on the emission.

5.2 Experiment

Nitrogen-doped diamond films were synthesized utilizing plasma-assisted chemical vapor deposition. The films were deposited on 1-in. Diameter polished molybdenum disks to obtain a low electrical resistance for the structure. To enhance the nucleation, the films were sonicated in a solution containing diamond particles and titanium particles and thoroughly rinsed to remove any large particles. The initial buffer layer with a high sp^2 density was synthesized using 400 sccm hydrogen and 8 sccm methane at a chamber pressure of 20 Torr, microwave power of 600 W and a

substrate temperature of 660°C. Next, a nitrogen-doped poly-crystalline diamond layer was grown using 400 sccm hydrogen, 2.5 sccm methane, 60–100 sccm nitrogen, at a chamber pressure of 50 Torr, a microwave power of 1300 W and a substrate temperature of 900°C. The final step was a 1-minute hydrogen/deuterium passivation, where the temperature was lowered to 650°C; the chamber pressure dropped to 20 Torr and the microwave power reduced to 600W. The film growth for each grow step was monitored by in situ laser interferometry.

The dysprosium (Dy) surfaces were prepared by e-beam evaporation of Dy (99.999%) onto a cleaned Si (001) surface (etched in HF just prior to loading into the vacuum loadlock). The deposition rate was monitored using a quartz crystal monitor. Prior to the deposition onto the substrate, approximately 50 Å of Dy was evaporated while a shutter covered the sample surface to remove contamination that might have accumulated on the source metal surface. The deposition rates of 1.0±0.2 Å per second was employed for a thickness of 100 nm. The base pressure of the system was $2 \cdot 10^{-10}$ torr while the pressure during deposition was less than $8 \cdot 10^{-9}$ torr

Thermionic emission spectra and temperature dependent UV photoemission spectra were measured in a UHV chamber with a base pressure of ~3×10^{-10} Torr, a sample heating stage, and a VSW-HA50 hemispherical analyzer. The temperature range of the measurements was limited to 600°C to avoid damage to the electron analyzer. The elevated sample temperature in the spectroscopy measurements was achieved by radiative heating from a tungsten coil filament mounted on a boron nitride disk behind the sample. A chromel–alumnel (K-type) thermocouple as well as optical pyrometer (MIKRON-M90Q) was employed to measure the sample surface temperature for temperatures above 250°C. Temperature measurements below 250°C were obtained by linear extrapolation of the thermocouple-pyrometer calibration

curve. The electron spectrometer was calibrated using an in situ deposited gold film, and measurements were obtained under UV irradiation (using HeI 21.2 eV emission) at temperatures up to 600°C. The UV photoemission spectra of the gold film did not show significant changes throughout the temperature range which served as a verification that magnetic fields generated in the heater filament did not affect the measurements.

To discern the temperature dependent emission properties, all spectroscopy measurements were performed with both increasing and decreasing temperature cycles. The electron multiplier was set to 2.7 kV. A negative 4 V bias was applied to the sample to overcome the work function of the analyzer. Both thermionic and UV photoemission spectra were obtained at elevated temperatures.

We note that the electron spectroscopy measurements and the metal deposition chambers were interconnected through a UHV sample transfer system to minimize effects due to surface contamination. The diamond films were grown in a separate chamber and were transferred into vacuum after a short exposure to ambient air, but these H-terminated surfaces were found to be less sensitive to surface contamination.

5.3 Results and Discussion

Ultraviolet photoemission spectroscopy (UPS) and thermionic emission spectroscopy (TES) were employed to determine the relation of the thermionic emission to the band energies of the diamond film. Fig 5.1 displays the ultraviolet photoelectron spectra and thermionic emission spectra of the N-doped CVD diamond at room temperature and at 500 °C. The UPS scans indicate that the surface exhibits a negative electron affinity at both 20 and 500 °C. The analysis involves determination of the width of the spectrum (W) and then using the expression $\chi = h\nu$ - W – E_g,

where $h\nu$ is the photon energy (21.2 eV), E_g is the band gap (5.4 eV), and W is the spectral width from the valence band maxim (VBM) to the low kinetic energy cut off (16.0 eV for both temperatures). In general, UPS cannot be used to indicate the value of the electron affinity unless there is sub-bandgap emission from surface states. Studies on natural crystal surfaces have suggested that the vacuum level is 1.2 eV below the conduction band[11, 12].

The same results can be used to determine the position of the surface Fermi level relative to the conduction band minimum. The results indicate that the Fermi level is 3.5 eV below the conduction band at room temperature which decreases to 2.5eV as the temperature is increased to 500 °C. We have previously ascribed this decrease to a combination of reduced band bending and the increase in the Fermi energy ascribed to semiconductor statistics[13, 14].

The TES is detected at 500°C and is also shown in Fig. 5.1. It is evident that the TES has the same low kinetic energy cut off at 2.4eV as is observed in the UPS. These results strongly support the proposal that the thermionic electron emission originates from the conduction band of the NEA diamond. The temperature dependent TES was observed at temperature starting at 323°C where thermionic emission spectra also had the cutoff at 2.5eV corresponds to an effective work function of approximately 2.5 eV and the intensity increased expotentially with temperature increasing, shown in the Fig 5.2.

Fig 5.3 depicted the UPS of Dy at room temperature and 600°C, both indicating metallic properties with potoelectron emission at Fermi level. The temperature don't showed apparent effect on the work function of 2.5eV. In Fig 5.4, thermionic emission spectra could be observed only when the Dy was heated up to 600°C, nearly 300°C higher than the emission from CVD diamond. The low kinetic energy cutoff

indicates the work function of 2.5 eV, consistant with the UPS determination.

Similar to the fitting method in the study of energy distribution of field emission[15-17], the experimental data were fitted by the convolution of P(E) and G(E), as $P(E) \otimes G(E)$. The instrument is assumed to have Gaussian transmission function[15-17] $G(E) = \frac{1}{\sqrt{2\pi}\Delta E_{FWHM}} \exp[-4\ln\sqrt{2}(\frac{E - E_c}{\Delta E_{FWHM}})^2]$, where E_c is the peak center of Gaussian function and ΔE_{FWHM} is the full width at half maximum (FWHM) of analyzer instrument. The thermionic emission energy distribution is under Maxwell-Boltzmann distribution[18] by $P(E) = C * E * \exp[\frac{-E}{k_B T}]$, where A is the Richarson constant, T is absolute temperature, Φ is the work function and k_B is the Boltzmann constant. In Fig 5.3, the measured FWHM of thermionic emission peak from Dy is 0.3eV. The fitted ΔE_{FWHM} =0.18eV is close to the equipment manual suggestion value of 0.15eV. The nature peak width 0.21eV is around 2.7k_BT for T=600^{o}C， comparing with the theoretical values of 2.45 k_BT[19]. However, In Fig 5.5, the measured FWHM of thermionic emission peak from CVD diamond is 0.2eV at 600^{o}C, 0.1eV narrower that the Dy peak with. Considering the same broaden effect by the same equipment, the data was fitted using the half-Maxwellian distribution[18, 20] $P(E) = C * E^{\frac{1}{2}} * \exp[\frac{-E}{k_B T}]$. The result of the nature peak width 0.13eV is around 1.7k_BT for T=600^{o}C, comparing with the calculations of FWHM=1.85k_BT for half-Maxwellian energy distribution.

One limiting phenomenon to the thermionic emission of electrons in the energy converter is the space charge effect[5], where emitted electrons had zero or low kinetic energy impede additional electron emission, shown in Fig 5.6(a). The negative space

charge will screen further thermionic electrons passing the vacuum space and reduce the output power density. The introduction of NEA to the diamond[10] semiconductor could mitigate this effect because the conduction band is more than 1eV above the vacuum level. Fig 5.6(b) depicted the half-Maxwellian thermionic emission from the conduction band minimum of semiconductor with negative electron affinity in band diagram. The thermionic electrons from conduction band will convert this potential energy to the kinetic energy in the vacuum and the velocity could reach 10^5 m/s if no scattering considered. Therefore, the transit time from the emitter to the electron collector is consistently reduced, accordingly reducing the space charge effects. Smith[21] etc. Had theoretically validated the negative electron affinity effect on the negative space charge effect reduction of a vacuum thermionic energy conversion device.

The transmission coefficient D(E) in the vacuum electron emission was defined in the equation[22] as $J = \int N(E)D(E)dE = \frac{4\pi mekt}{h^3}\overline{D}(E)\int \exp(-\frac{E-\Phi}{kT})dE$, where J is the emission current density, N(E) is the density of states (DOE) and $\overline{D}(E)$ is the effective transition coefficient. For typical semiconductors or metals with work function of Φ, the effective transition coefficient $\overline{D}_1(E)$ was represented[22] as $\overline{D}_1(E) = 4\sqrt{\frac{kT}{\Phi}}\int_0^\infty \sqrt{x}(1-4\sqrt{\frac{kTx}{\Phi}}+\frac{17}{2}\frac{kTx}{\Phi}-...)e^{-x}dx$; While considering the vacuum level is ~1eV (χ) below the conduction band minimum and the dipole layer thickness is l ~1.5Å, the effective transition coefficient $\overline{D}_2(E)$ for NEA material can be derived via quantum mechanics as[22] $\overline{D}_2(E) \approx 8\sqrt{\pi}\frac{(kT\Phi)^{1/2}}{\Phi-\chi}\exp(-2al\sqrt{\chi})$. At this NEA case, electron emissions could happen below the conduction band level because electron

wave functions could transmit through the thin energy barrier at surface. At the conditions when work function is 1.6eV and temperature is 600°C, $\overline{D}_2(E)$ was calculated to be 0.51 and $\overline{D}_1(E)$ correspond to 0.25. Fig 5.7 illustrates the negative electron affinity on the transmission coefficient of the thermionic emission from semiconductor. This calculation is consistent with the experiment observations of emissions below the conduction band (discussions in Chapter 3 and Chapter 4). This emissions increase with the temperature increasing and finally smear the liner fitting of low kinetic energy cutoff at the conduction band at high temperature condition.

It is noted that the thermionic emission current from N-doped CVD diamond is observed to be increasing as the top diamond thickness decreasing. This phenomenon was attributed to the electron kinetic energy loss by the inelastic scattering in the transport in the conduction band. For NEA semiconductors, electrons at the conduction band minimum of a semiconductor transport by the diffusion, not the hot electron transport[23]. The diffusion length is usually longer than the thermal length to prevent the electron kinetic energy loss during inelastic collisions and increasing electron yield in the emission. Several values of crystal or CVD diamond diffusion length ranging from several to hundred micrometer were reported[23-25]. However, our sample is composed of large nitrogen impurities and sp^2 components at top diamond layer, which would significantly reduce the diffusion length of electrons. The tradeoff between doping and diffusion length need to be optimized by the growth processing.

5.4 Conclusion

The TES of Dy and N-doped Diamond with the similar 2.5eV work function were compared to elucidate the effect of a NEA on thermionic emission. With the same work function, thermionic emission from diamond with NEA was detected at

much lower temperature than the Dy. The negative electron affinity results in thermionic emission that originates from the conduction band minimum of the diamond. The peak width of TES from NEA diamond is narrower that that from Dy. Fitting results showed thermionic emission from Dy follows the traditional Maxwell-Boltzmann distribution while the thermionic emission CVD diamond is more close to the half-Maxwellian distribution. The NEA effect on the thermion emission properties was also discussed considering the space charges and transmission coefficient.

5.5 Reference

1 B. F. Williams and J. J. Tietjen, Proceedings of the Institute of Electrical and Electronics Engineers **59**, 1489 (1971).

2 S. Iannazzo, Solid-State Electron. **36**, 301 (1993).

3 N. S. Rasor, J. Appl. Phys. **31**, 163 (1960).

4 P. G. Tanner, D. A. Fraser, and A. D. Irving, IEE Proc.-Sci. Meas. Technol. **152**, 1 (2005).

5 C. Herring and M. H. Nichols, Rev. Mod. Phys. **21**, 185 (1949).

6 F. A. M. Koeck and R. J. Nemanich, Diam. Relat. Mat. **15**, 217 (2006).

7 F. A. M. Kock, J. M. Garguilo, and R. J. Nemanich, Diam. Relat. Mat. **10**, 1714 (2001).

8 S. A. Kajihara, A. Antonelli, J. Bernholc, and R. Car, Phys. Rev. Lett. **66**, 2010 (1991).

9 R. G. Farrer, Solid State Commun. **7**, 685 (1969).

10 J. Vanderweide, Z. Zhang, P. K. Baumann, M. G. Wensell, J. Bernholc, and R. J. Nemanich, Phys. Rev. B **50**, 5803 (1994).

11 J. B. Cui, J. Ristein, and L. Ley, Phys. Rev. Lett. **81**, 429 (1998).

12 B. Rezek, C. Sauerer, C. E. Nebel, M. Stutzmann, J. Ristein, L. Ley, E. Snidero, and P. Bergonzo, Appl. Phys. Lett. **82**, 2266 (2003).

13 A. T. Collins, J. Phys.-Condes. Matter **14**, 3743 (2002).

14 J. S. Blakemore, *Semiconductor Statistics*, 1987).

15 R. Schlesser, M. T. McClure, W. B. Choi, J. J. Hren, and Z. Sitar, Applied Physics Letters **70**, 1596 (1997).

16 R. D. Young and C. E. Kuyatt, Review of Scientific Instruments **39**, 1477 (1968).

17 C. Bandis and B. B. Pate, Appl. Phys. Lett. **69**, 366 (1996).

18 A. Modinos, *Field, Thermionic, and Secondary Electron Emission Spectroscopy* (Plenum, New York, 1984).

19 R. D. Young, Physical Review **113**, 110 (1959).

20 A. R. Hutson, Physical Review **98**, 889 (1955).

21 J. R. Smith, G. L. Bilbro, and R. J. Nemanich, Diam. Relat. Mat. **15**, 2082 (2006).

22 A. L. Reimann, *Thermionic emission* (Wiley, 1934).

23 J. Ristein, W. Stein, and L. Ley, Phys. Rev. Lett. **78**, 1803 (1997).

24 T. Teraji, S. Yoshizaki, S. Mitani, T. Watanabe, and T. Ito, J. Appl. Phys. **96**, 7300 (2004).

25 Y. V. Pleskov, A. Y. Sakharova, E. V. Kasatkin, and V. A. Shepelin, J. Electroanal. Chem. **344**, 401 (1993).

26 H. Lüth, *Interfaces and Thin Films. 3rd* (Springer, 2001).

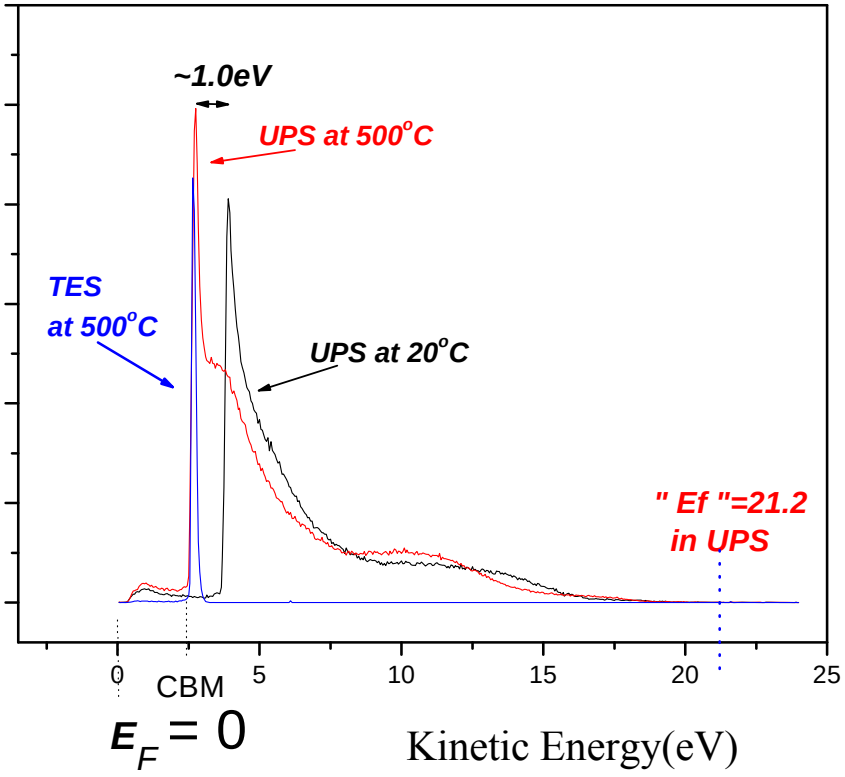

Fig 5.1 Ultraviolet photoelectron spectroscopy and thermionic emission spectroscopy of N-doped diamond showing the thermionic emission from the CBM

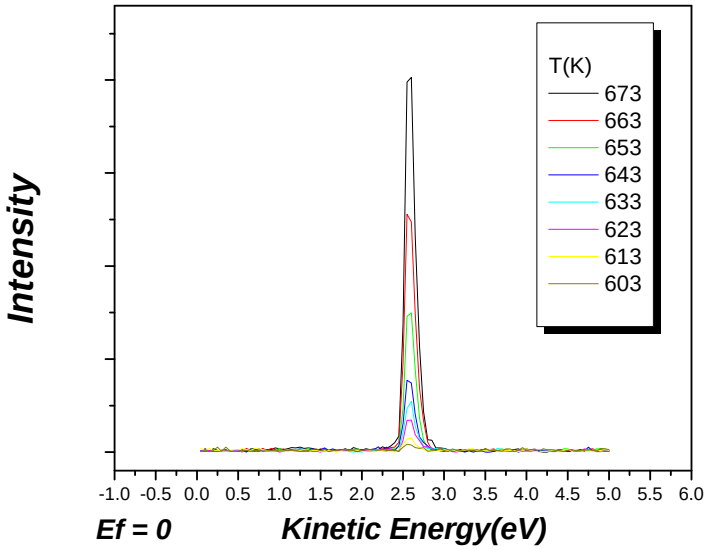

Figure 5.2 Thermionic emission spectroscopy was observed from N-doped diamond starting at 603K.

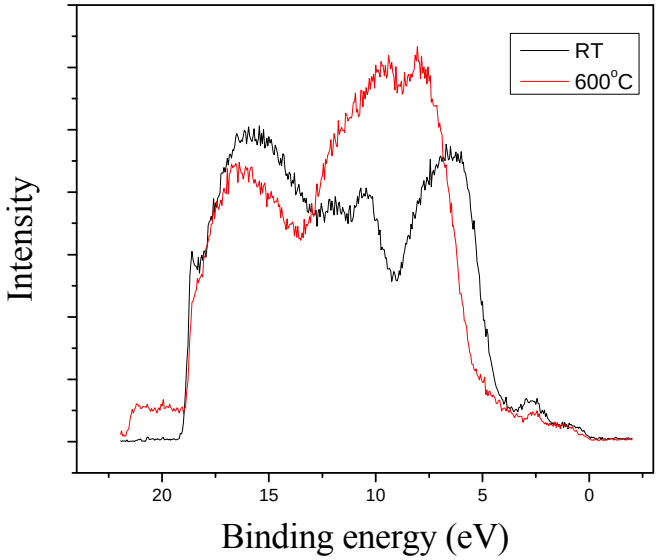

Fig 5.3 Ultraviolet photoelectron spectroscopy and thermionic emission spectroscopy of Dy showing the metallic properties and 2.5eV work function.The temperature don't have effect on the work function.

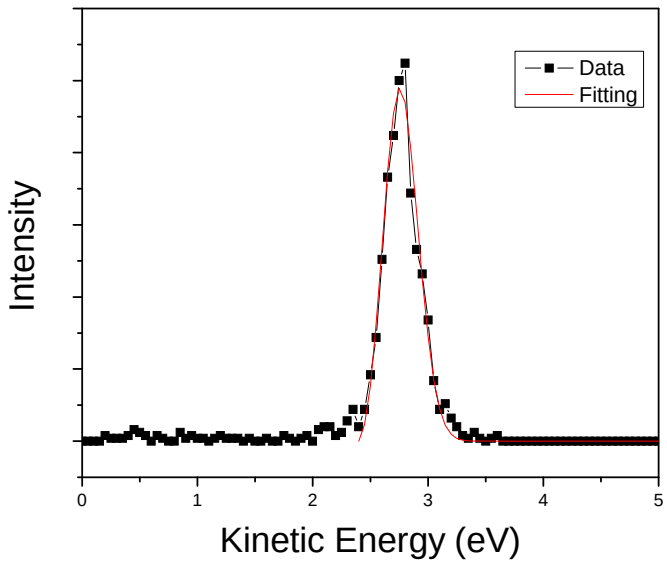

Figure 5.4 Thermionic emission spectroscopy was observed from Dy at 600^{o}C and the fitting results indicate 2.7k_BT natural peak width.

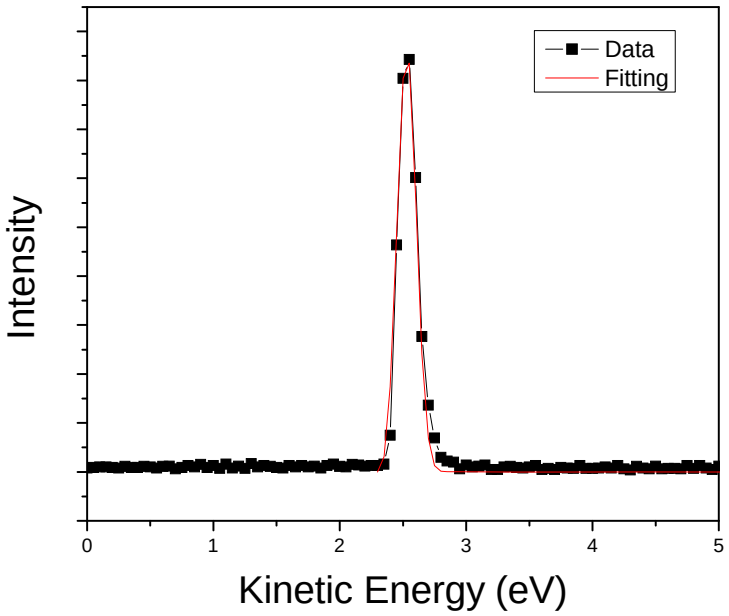

Figure 5.5 Thermionic emission spectroscopy was observed from CVD diamond at 600^{o}C and fitting results indicate 1.7k_BT natural peak width.

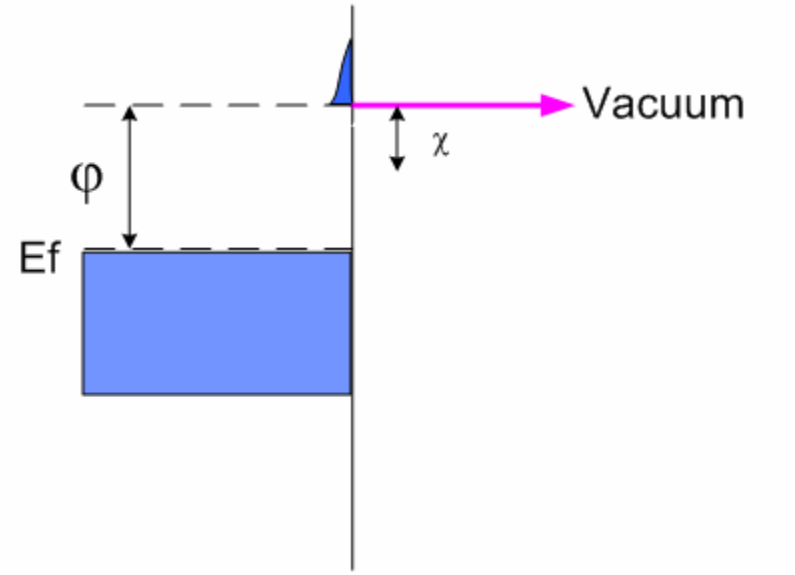

(a)

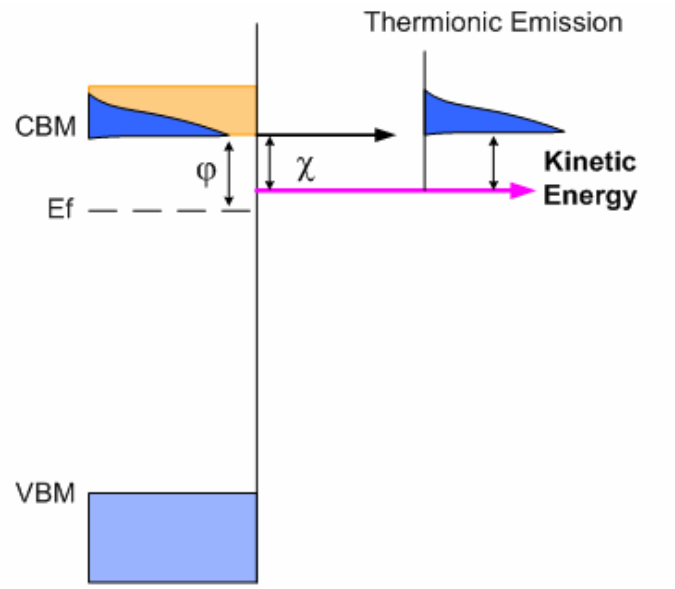

(b)

Figure. 5.6 Schematic diagrams of (a) the thermionic emission from vacuum level with Maxwell-Boltzmann energy distribution for Dy metal and (b) the thermionic emission from conduction band with Half-Maxwellian energy distribution for diamond semiconductor with negative electron affinity.

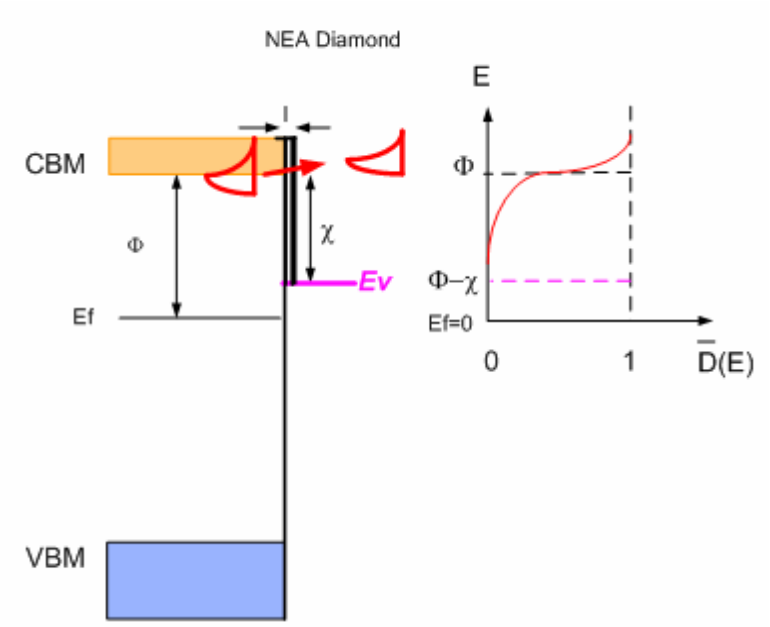

(a)

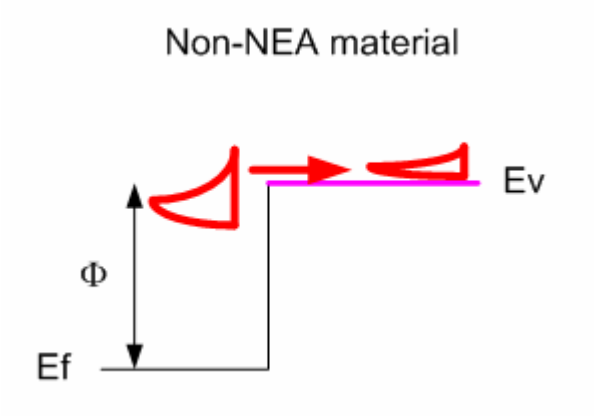

(b)

Fig 5.7 the schematic of the transition coefficient of the thermionic emission from (a) semiconductor with negative electron affinity and (b) non-NEA material.

6. Polarity Effects on the Surface Properties of AlGaN

Y. J. Tang, J-S. Park, R.F. Davis and R. J. Nemanich

Department of Physics and Materials Science and Engineering,

North Carolina State University,

Raleigh, NC 27695-8202

Abstract

N-polar and Al (Ga)-polar AlGaN films were grown on C-polar and Si-polar SiC substrates, respectively. Atomic Force Microscopy images of the surfaces after KOH etching verified the N-polar face which is highly reactive and showed etch pits while the Al-face was resistant to KOH etching. Combined XPS and UPS characterization have shown that both N-polar and Al-polar surfaces of AlN have a zero or negative electron affinity. Furthermore, it has been determined that the N-face AlN has a lower work function (2.5eV) than the Al-face AlN (3.0 eV). The difference is attributed to the spontaneous polarization field. The results for the AlGaN alloy surfaces indicate that as the Al concentration is increased, the electron affinity and work function decreases. However, the band bending increases.

6.1 Introduction

Recent studies have indicated that III-nitride semiconducting materials[1, 2] may be appropriate as a material for field emission cathodes with applications in high power microwave tubes or vacuum microelectronics and for thermionic cathodes with possible application in thermionic energy conversion structures. The advantages[3] of these materials for electron emission is due to its high melting point, high thermal conductivity, chemical stability, n-type doping, and low or negative electron affinity (NEA)[4-6]. For a material that exhibits a NEA, electrons at the conduction band minimum can be emitted into vacuum without being bound by an energy barrier at surface. Moreover, the combination of efficient n-type doping and a negative electron affinity should result in low work function surfaces appropriate for thermionic emission.

Additionally, III-nitrides are also piezoelectric as well as pyroelectric due to its non-symmetric wurtzite structucture.[7, 8] the spontaneous polarizations anticipated for GaN and AlN are P_{SP} =-0.034; and -0.090 C/m^2, respectively, and consequently the surface will exhibit a polarization bound charge of the same magnitude. The polarization bound charges can result in electric field which affect the band bending and carrier dynamics near the surface. The polarization bound charge of the Al or Ga surface is negative while the polarization bound charge for the N-polar is positive. In this study, the effects of the polarization on the surface properties are studied with photoemission spectroscopy. The particular focus of this study is determining whether the polarization bound charge can be employed to reduce the work function of the surfaces to achieve enhanced electron emission.

It has been shown that for III-nitride epitaxial semiconducting films grown on polar (0001) or (000-1) 6H SiC surface results in III or N-polar surfaces, respectively. The observation is attributed to the preference for Si-N or C-III interface bonding, which has been predicted theoretically[9-12] and observed experimentally[12-16]. Harada et al. reported that the AlN films grown on Si/C-polar SiC have shown Al/N polar surfaces. Gogneau et al.[16] have verified that N-polar AlN was grown on (000-1) 6H SiC substrates and further investigated the growth mode of N-face GaN.

In this study, polar AlGaN films grown on Si/C-polar SiC substrates were investigated with Atomic Force Microscopy (AFM), Ultraviolet Photoemission Spectroscopy (UPS) and X-ray Photoemission Spectroscopy (XPS).

6.2 Experimental

The $Al_xGa_{1-x}N$ films were grown by Metal-Organic Vapor Phase Epitaxy (MOVPE) using a cold-walled, vertical, pancake-style system. The on-axis, n-type 6H-SiC substrates were etched in an HF:H_2O (1:10) solution for 10 min at room temperature, rinsed in de-ionized water, and blown dry with nitrogen prior to loading into the growth reactor. Trimethylaluminum (TMA), triethylgallium (TEG), and ammonia were used as the precursors; hydrogen served as both the carrier and the diluent gas. The reactor pressure was fixed at 20 Torr for the growth of all films. The 100nm-thick $Al_xGa_{1-x}N$ ($0 < x \leqslant 0.61$) layer was grown on a 100nm-thick Si-doped $Al_{0.15}Ga_{0.85}N$ buffer layer, which was optimized for growth directly on the SiC substrates. The 10nm thick $Al_{0.8}Ga_{0.2}N$ and AlN layers were directly deposited on the on-axis (0001)/(000-1) 6H-SiC substrates for the purpose of the photoemission study.

The reactor pressure was fixed at 20 Torr, and the growth temperature was 1100°C. The molar flow rate of SiH_4 was kept constant at 1.43 mol/min, and resulted in a GaN film doped with Si at a concentration of approximately 1 x 10^{19} cm^{-3}. The value of ionized donor concentration, N_D–N_A, decreased with increasing mole fraction of Al in the $Al_xGa_{1-x}N$ alloy films, and the donor concentration was below the detection limit (~1 x 10^{17} cm^{-3}) of the C-V equipment for $x > 0.60$.

Atomic Force Microscopy (AFM) using a Park Scientific Instruments Autoprobe M5 system was employed to examine the morphology of the surfaces before and after the 10 min KOH (22.5%) etching process. This approach was employed to verify the polarity of the surface. The scans were acquired over a 1 μm x 1 μm region using a probe with a silicon tip.

The surfaces were cleaned ex-situ using a wet chemical process and in situ using a chemical vapor cleaning (CVC) process. Prior to in situ processing, the samples were immersed in TCE, acetone, and methanol for 2 min; then dipped in in 37% hydrochloric acid (HCl) for 10 min, in a 1:10 HF:H_2O solution for 5mins and in de-ion.zed water for 5mins remove the oxide and hydroxide. For the CVC process, blue ammonia was introduced via a leak valve into the GSMBE when the thermocouple temperature reached 500 °C and the sample surface temperature was held 20 mins at 850-1100°C for the different Al concentration in AlGaN. The chamber was maintained at an ammonia pressure of $(1.0 \pm 0.1)*10^{-4}$ Torr during the CVC process. The surface temperature of the sample under annealing was measured using an Ircon Ultimax infrared thermometer with an emissivity setting of 0.5. Experimental procedures are identical to previous studies in our lab[17, 18]. After the chamber pressure<$2.0*10^{-8}$ Torr, the samples were transferred in situ to XPS and then UPS

chambers for measurements. The pressure of the transfer line was typically ,8*10^{-10} Torr.

X-ray photoemission spectra were obtained at a pressure of 2 x 10^{-9} Torr using the 1253.6 eV Mg Kα or the 1486.6 eV Al Kα lines from a VG Microtech XR3 dual anode source and a VG Microtech Clam II electron analyzer. The resolution of the analyzer was determined from the full width at half maximum (FWHM) of the gold 4f 7/2 spectral peak to be approximately 1.0 eV. Through curve fitting, the centroid of spectral peaks can be resolved to ±0.1 eV. The settings for the x-ray source were 5 A filament current, 20 mA emission current, 13 kV accelerating voltage, and 3.0 kV channeltron voltage. Survey scans and core level spectra were collected using pass energies of 50 and 20 eV, respectively. A linear background was subtracted from the core level spectra, and the resulting spectra were fitted with a mix of Gaussian–Lorentzian functions.

UV Photoemission Spectroscopy (UPS) was employed to measure the electronic states near the valence band and to determine the electron affinity and work function. An Omicron HIS13 discharge lamp was employed and optimized to generate a maximum amount of He I (21.2 eV) radiation and to minimize the amount of He II (40.8 eV) radiation. The lamp voltage and discharge current were set to 520 V and 50 mA, respectively. The electron multiplier was set to 2.6 kV, and a pass energy of 15 eV was used. The resolution of the 50 mm mean radius hemispherical analyzer was approximately 0.1 eV. A negative 4 V bias was applied to the sample to overcome the work function of the analyzer.

In photoemission studies of wide band gap materials, charging can be a problem. Charging effects are typically manifested in two ways: (1) a shift of the spectra shift

to higher binding energy which is due to a change in system bias[19]; or (2) the spectra are distorted such that the width (W) is compressed. The first affect would result in an error in the work function and the second affect would result in an error in the determination of the electron affinity. To avoid these charging effects, the samples employed in this study were doped with Si and a very thin layer was employed for the AlN layers[19, 20] .

6.3 Results and Discussion

6.3.1 AlN films

The combination of KOH etching and AFM measurements were employed to confirm the polarity of the grown surfaces. Figure 6.1 shows the AFM images of the surfaces of AlN grown on Si- face and C-face SiC. Images are presented before and after the 10 min KOH (22.5%) etching process. For the the AlN film grown on Si-face SiC, the surface morphology before (Figure 6.2 (a)) and after (Figure 6.2 (b)) etching exhibits a smooth surface which remained essentially unchanged after KOH etching indicating an Al-polar surface. These results are consistent with studies of wet etching on polar GaN,[21-23] where the surface is resistant to KOH etching. In contrast, for AlN grown on C-face SiC, comparison of the AFM images prior to etching (Figure 6.2 (c)) with that after etching (Figure 6.2 (d)) shows a significant change in the surface morphology. It is apparent that this surface is highly reactive to exposure in the KOH solution. The highly selective etching properties of III-Nitride polar surface has been attributed to the properties of the nitrogen atomic configurations which are exposed on the N-polar surface[23].

Fresh sections of the samples were then chemically cleaned, mounted on a molybdenum sample plate, and loaded into UHV. The samples were transferred into a gas source MBE for the chemical vapor cleaning process. After cleaning the substrates were transferred in UHV to the XPS chamber for chemical analysis.

To explore the band energies of the two surfaces, the X-ray photoemission spectroscopy of the Al 2p core level was carefully measured for both faces, and the results are shown in Fig 6.3 (a). It is evident that the N-polar AlN exhibits a peak position which is shifted by 0.6 eV to higher binding energy compared with the Al face. Generally, it can be assumed that the energy difference between a core level and the valence band maximum should be constant independent of the surface orientation and termination. In the energy alignment diagram Fig 6.3 (b), it is evident that the surface Fermi level of the N-face AlN is increased by 0.6eV as compared with the Al-polar AlN. In both cases the Fermi level falls in the middle of the gap even though the samples were doped with Si in an attempt to achieve n-type character at the surface.

Figure 6.4 shows ultraviolet photoemission spectroscopy of the Al/N polar AlN surfaces. The electron Affinity and work function can be determined from the spectral width (W) which is the energy difference from the low energy cutoff to the emission from the valence band maximum. The semiconductor electron affinity (χ) and work function (Φ) can be expressed as $\chi = h\nu - E_g - W$ and $\Phi_s = h\nu - E_g - (E_F - E_v)$.

The spectrum width is determined from the low energy cutoff, which can be determined with the precision of the spectromter, and the high energy cut-on which is representative of the valence band maximum (VBM). The weak signal at the VBM is the largest uncertainy in this analysis. In this study we have fit the leading edge of the spectrum with two straight lines and extrapolated the leading one to zero emission. As

indicated in Fig. 6.4a the low energy cut off is at 3.8 eV and the VBM from the extrapolation is at 18.7 eV. The spectrum width, W, is then 14.9±0.2 eV. Thus, the electron affinity χ is calculated to be 0.1±0.2 eV (= 21.2 eV– 6.2 eV – 14.9±0.2 eV). This result is in essential agreement with two prior reports, Ward et al.[19] and Graboski et al.[6], but they are inconsistent with a measurement that has shown an electron affinity of greater than 1.5 eV[24, 25]. It has also been noted that the presence of oxygen on the surface can significantly affect the measured electron affinity[6].

The measurements can be used to determine the postion of the Fermi level at the surface and also the work function. As indicated in Figure 6.4 a, the low energy cutoff is at 3.8 eV which suggests that the conduction band minimum is at 24.9 eV (i.e. 3.7 eV + 21.2 eV). The Fermi energy is at 0.7 eV and correspondingly at 21.9 eV indicating that the CBM is 3.0 eV above the Fermi energy. The extrapolation of the leading edge indicates the valence band maximum at 18.7 eV which is 3.2 eV below the Fermi level. In this case the work function for the Al-polar AlN is 3.0eV.

The N-polar AlN was analyzed using the same procedures. The spectrum displays a width, W, of 14.9±0.2 eV with a low energy cutoff at 3.3 eV and a VBM at 18.2±0.2 eV. Again the electron affinity is found to be 0.1±0.2 eV for the ammonia cleaned surface indicating that both the N-polar and Al-polar AlN exhibit a similar nearly zero electron affinity. The Fermi level in this case is 3.7 eV above the VBM and 2.5 eV below the CBM which implies that the binding energy of the valence band is 0.5±0.2 eV deeper for the N-polar surface. These results are in essential agreement with the XPS measurements were the Al 2p core level was 0.6eV lower for the N-face relative to that from the Al-face.

Both Al-polar and N-polar surfaces of AlN epitaxial films exhibit a similar electron affinity, but they show a work function difference of ~0.5 eV. This

experiment result is displayed schematically in Fig 6.5. We consider two effects that could contribute to the observation of a change in the work function: 1) the polarity effect through the polarization bound charge, and 2) different band alignment to the substrate originating from the different interface bonding. Considering first the polarization, the spontaneous polarization is oriented from the Ga-face towards the N-face, producing negative bound charges on the Al-face (0001) and positive bound charges on the N-face (000-1). Negative charges will result in the upward band bending at surface while positive bound charges would generate downward band bending. The difference 0.4-0.6eV is consistent with our experiment results. Solving Poisson equation $d^2V/d^2z=\rho/\varepsilon_r\varepsilon_0$, where V is potential, z is thickness, ρ is charge density, ε_r is material dielectric and ε_0 is vacuum permittivity, the potential difference ΔV is calculated to be 1.2 eV where $\rho=0.090$ C/m^2 and the thickness 10 nm. Next we consider the effects of the band alignment at the interface of the SiC and AlN. A previous study has reported[26] that AlN/SiC had valence band offset of ΔE_v=1.1-1.2eV for metal-polar and ΔE_v=0.6-0.7eV for the N-polar interface.

6.3.2 AlGaN alloys

A series of Si-doped $Al_xGa_{1-x}N$ samples was prepared on Si-polar and C-polar SiC substrates. The values of the bandgap energies, E_g, of the solid solutions of concern were determined from the wavelengths of the respective peaks of the bandedge emission acquired via cathodoluminescence (CL) measurements conducted at with the samples at room temperature. The Al mole fraction, x, of the various compositions of the $Al_xGa_{1-x}N$ layers was calculated using $E_g(Al_xGa_{1-x}N) = x \cdot E_g(AlN) + (1–x) \cdot E_g(GaN) – b \cdot x \cdot (1–x)$. The band gaps of GaN and AlN at room

temperature are 3.4 and 6.2 eV, and the bowing parameter, b, was assumed to be zero. All samples were cleaned in the gas source MBE using the ammonia exposure process. The samples were then transferred in UHV to the XPS chamber for chemical analysis. The C and O levels were less than 0.5% and 3% respectively for each of the samples.

For each alloy concentration, the N-polar shows a slightly lower electron affinity and significantly lower work function. For the samples with $x<0.6$, we can presume that the Fermi level in the bulk is near the conduction band edge. Therefore, the band gap energy minus the position of the Fermi level gives the upward band bending for each sample. Figure 6.6 depicts the electron affinity, work function and band bending of the $Al_xGa_{1-x}N$ alloys as a function of aluminum percentage. For the same Al content, the N-polar shows the lower electron affinity, work function, and band bending, comparing with Al-polar face.

Both of electron affinity and work function were observed to decrease with increasing Al percentage. However, band bending increase with Al percentage increasing, resulting in the work function didn't decrease too much. The expected the downward band bending on the N-polar surface could be compensated by the upward band bending at the surface may happen because of the surface charges[27] which could be induced by both the polarity and the oxygen contamination related surface states..

6.4 Conclusions

In conclusion, N/Al- polar AlN films grown on substrates of C/Si- polar SiC by MOVPE were confirmed first time by selective etching and AFM imaging. Combined XPS and UPS characterization have shown that both N-polar and Al-polar AlN epitaxial films on SiC have a nearly zero electron affinity. Furthermore, it have been determined that the N-face AlN has increased Fermi level in the Band-gap (E_c-

E_f=2.4eV) than Al-face AlN (E_c-E_f =3.0eV) at the surface due to the built in polarization field. From the AlGaN results, the electron affinities are close for each of polar surfaces. AlGaN shows the electron affinity and work function decrease, but band bending increase, with increasing Al percentage.

This work is supported by the Office of Naval Research (ONR) under the Thermionic Energy Conversion (TEC) - Multidisciplinary University Research Initiative (MURI) project.

6.5 References

[1] Y. Taniyasu, M. Kasu, and T. Makimoto, Appl. Phys. Lett. **85**, 4672 (2004).

[2] A. T. Sowers, J. A. Christman, M. D. Bremser, B. L. Ward, R. F. Davis, and R. J. Nemanich, Appl. Phys. Lett. **71**, 2289 (1997).

[3] V. V. Zhirnov, G. J. Wojak, W. B. Choi, J. J. Cuomo, and J. J. Hren, J. Vac. Sci. Technol. A-Vac. Surf. Films **15**, 1733 (1997).

[4] M. C. Benjamin, C. Wang, R. F. Davis, and R. J. Nemanich, Appl. Phys. Lett. **64**, 3288 (1994).

[5] M. C. Benjamin, M. D. Bremser, T. W. Weeks, S. W. King, R. F. Davis, and R. J. Nemanich, Appl. Surf. Sci. **104**, 455 (1996).

[6] S. P. Grabowski, M. Schneider, H. Nienhaus, W. Monch, R. Dimitrov, O. Ambacher, and M. Stutzmann, Appl. Phys. Lett. **78**, 2503 (2001).

[7] F. Bernardini, V. Fiorentini, and D. Vanderbilt, Phys. Rev. B **56**, 10024 (1997).

[8] O. Ambacher, et al., J. Appl. Phys. **87**, 334 (2000).

[9] J. C. Zheng, H. Q. Wang, A. T. S. Wee, and C. H. A. Huan, Appl. Phys. Lett. **79**, 1643 (2001).

[10] S. Y. Ren and J. D. Dow, Appl. Phys. Lett. **69**, 251 (1996).

[11] R. B. Capaz, H. Lim, and J. D. Joannopoulos, Phys. Rev. B **51**, 17755 (1995).

[12] F. A. Ponce, C. G. VandeWalle, and J. E. Northrup, Phys. Rev. B **53**, 7473 (1996).

[13] E. Monroy, E. Sarigiannidou, F. Fossard, N. Gogneau, E. Bellet-Amalric, J. L. Rouviere, S. Monnoye, H. Mank, and B. Daudin, Appl. Phys. Lett. **84**, 3684 (2004).

[14] J. Lu, L. Haworth, D. I. Westwood, and J. E. Macdonald, Appl. Phys. Lett. **78**, 1080 (2001).

[15] M. Harada, Y. Ishikawa, T. Saito, and N. Shibata, Jpn. J. Appl. Phys. Part 1 - Regul. Pap. Short Notes Rev. Pap. **42**, 2829 (2003).

[16] N. Gogneau, E. Sarigiannidou, E. Monroy, S. Monnoye, H. Mank, and B. Daudin, Appl. Phys. Lett. **85**, 1421 (2004).

[17] W. J. Mecouch, B. P. Wagner, Z. J. Reitmeier, R. F. Davis, C. Pandarinath, B. J. Rodriguez, and R. J. Nemanich, J. Vac. Sci. Technol. A **23**, 72 (2005).

[18] K. M. Tracy, P. J. Hartlieb, S. Einfeldt, R. F. Davis, E. H. Hurt, and R. J. Nemanich, J. Appl. Phys. **94**, 3939 (2003).

[19] B. L. Ward, J. D. Hartman, E. H. Hurt, K. M. Tracy, R. F. Davis, and R. J. Nemanich, J. Vac. Sci. Technol. B **18**, 2082 (2000).

[20] G. Martin, S. Strite, A. Botchkarev, A. Agarwal, A. Rockett, H. Morkoc, W. R. L. Lambrecht, and B. Segall, Appl. Phys. Lett. **65**, 610 (1994).

[21] A. R. Smith, R. M. Feenstra, D. W. Greve, M. S. Shin, M. Skowronski, J. Neugebauer, and J. E. Northrup, Appl. Phys. Lett. **72**, 2114 (1998).

[22] D. Huang, P. Visconti, K. M. Jones, M. A. Reshchikov, F. Yun, A. A. Baski, T. King, and H. Morkoc, Appl. Phys. Lett. **78**, 4145 (2001).

[23] D. S. Li, M. Sumiya, S. Fuke, D. R. Yang, D. L. Que, Y. Suzuki, and Y. Fukuda, J. Appl. Phys. **90**, 4219 (2001).

[24] C. I. Wu and A. Kahn, Appl. Phys. Lett. **74**, 546 (1999).

[25] C. I. Wu, A. Kahn, E. S. Hellman, and D. N. E. Buchanan, Appl. Phys. Lett. **73**, 1346 (1998).

[26] S. W. King, E. P. Carlson, R. J. Therrien, J. A. Christman, R. J. Nemanich, and R. F. Davis, J. Appl. Phys. **86**, 5584 (1999).

[27] H. Lüth, *Interfaces and Thin Films. 3rd* (Springer, 2001).

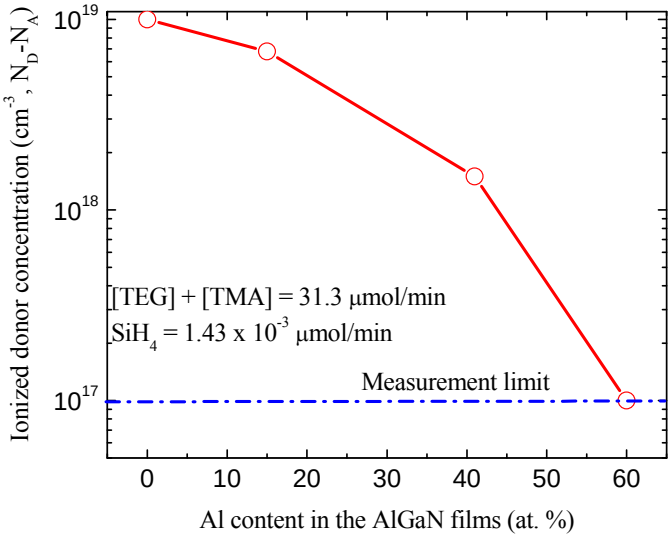

Figure 6.1 Ionized donor concentration, N_D-N_A, as a function of Al mole fraction in $Al_xGa_{1-x}N$ films. The SiH_4 flow rate was held constant at 14.3 nmol/min.

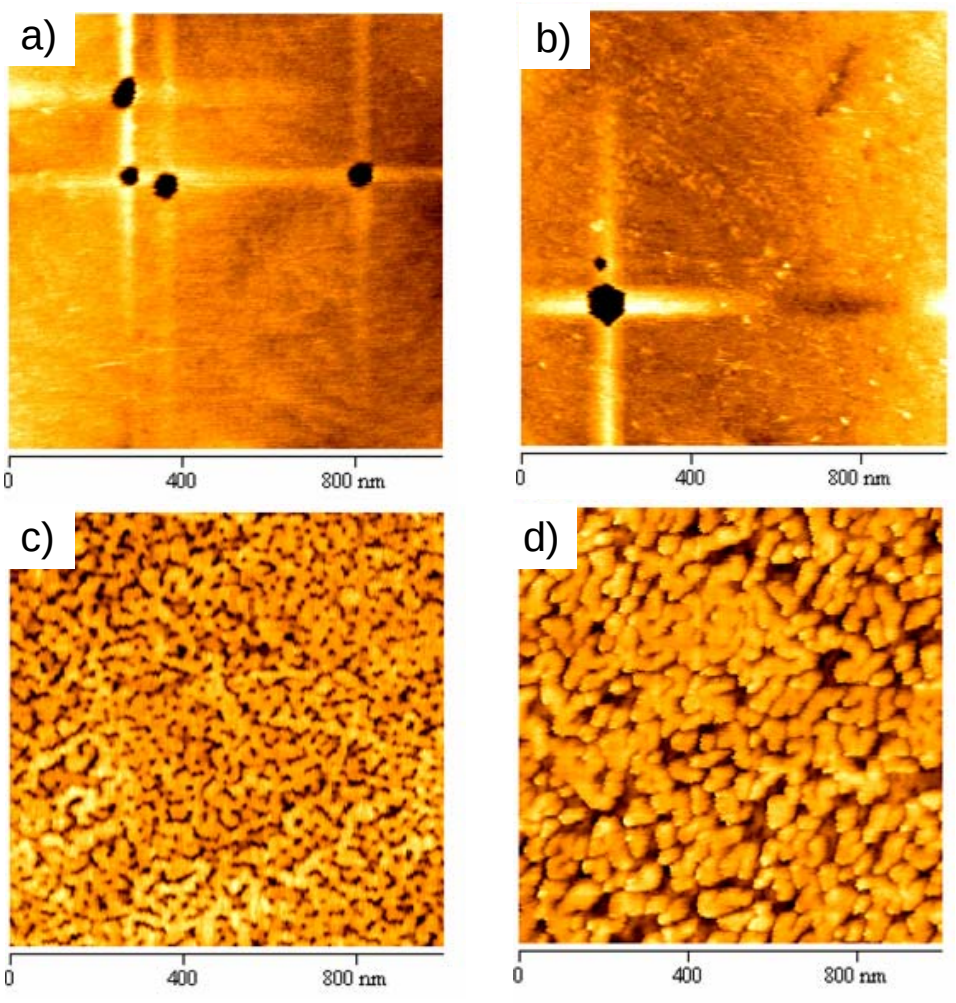

Figure 6.2 The AFM images of the surfaces of the AlN grown on Si- face and C-face SiC before and after KOH (22.5%) etching for 10 min respectively. There is no change in the surface morphology of AlN grown on the Si-polar SiC before (a) and after (b) etching, indicating the Al polar surface propweties. The film of AlN grown on the C-polar SiC is highly reactive with the KOH solution before (c) and after (d) etching, showing the N-polar surface properties.

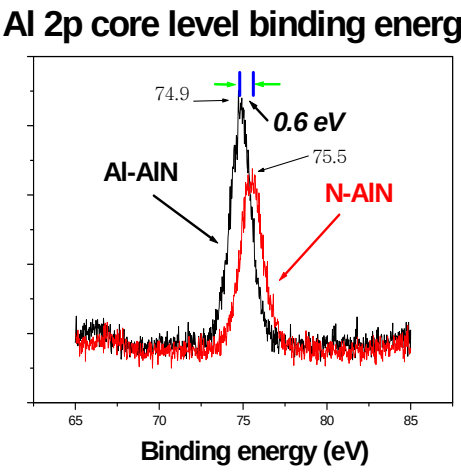

(a)

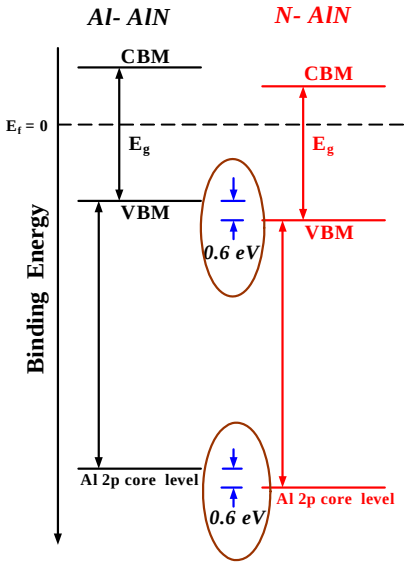

(b)

Figure 6.3 (a) X-ray photoemission spectroscopy of the Al 2p core level from N-polar and Al-polar AlN. The peak of the N-polar surface is shifted by 0.6 eV to higher binding energy compared with the Al-polar surface. (b) A schematic of the bands of N-polar and Al-polar AlN to reflect the 0.6eV difference in core level binding energy..

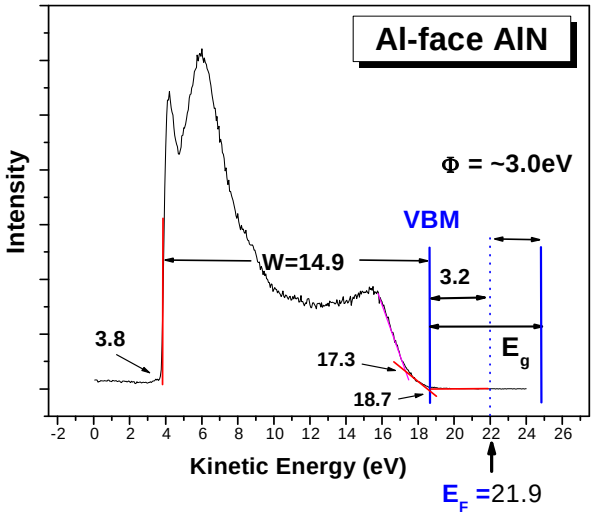

(a)

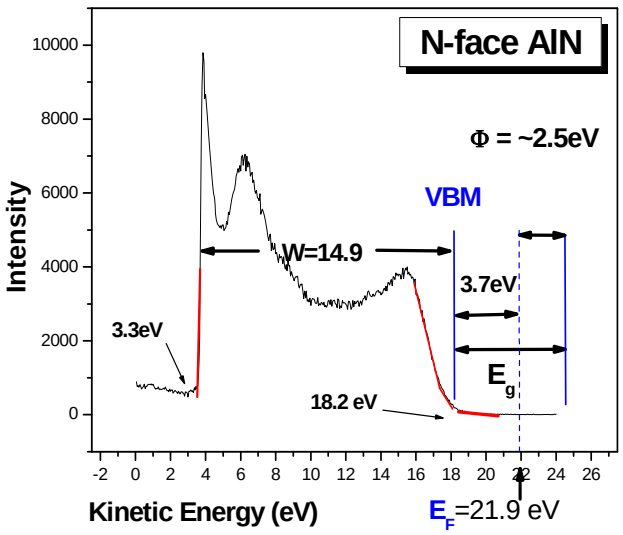

(b)

Figure 6.4 (a) Ultraviolet photoemission spectroscopy of Al polar AlN surface indicate 3.0 eV work function and negative electron affinity. (b) UPS of N polar AlN surface show2.5eV work function and negative electron affinity.

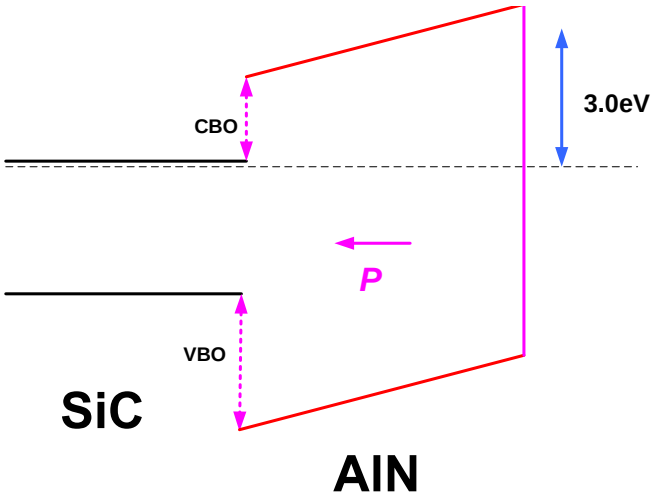

(a)

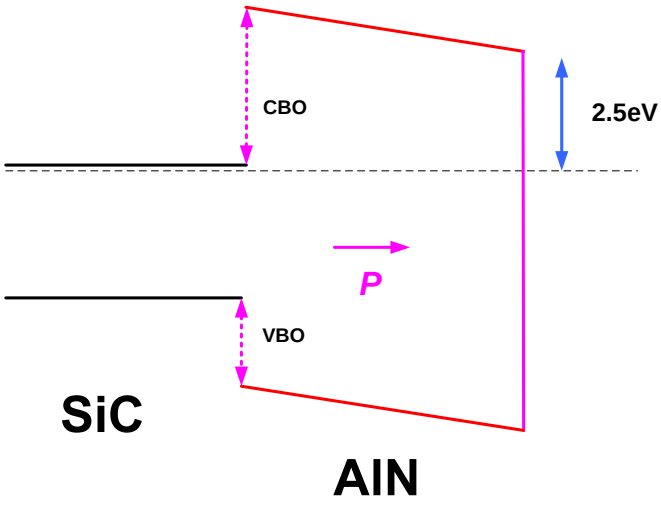

(b)

Figure 6.5 Band diagrams show (a) the Al-polar AlN/SiC have upward band bending and 3.0 eV work function and (b) the N-polar AlN/SiC have downward band bending and 2.5 eV work function.

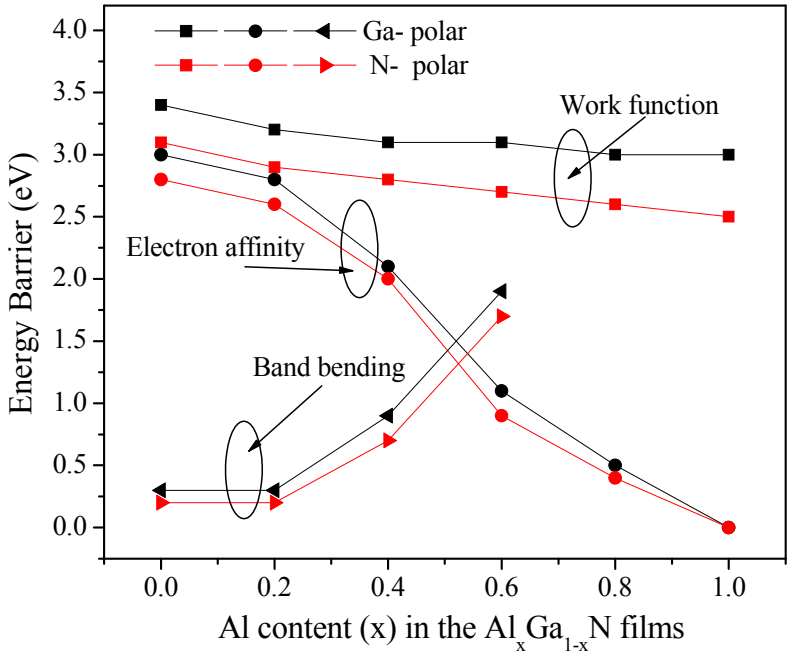

Figure 6.6 the electron affinity, work function and band bending as a function of aluminum percentage of the AlGaN alloy epitaxial films grown on C-polar and Si-polar 6H-SiC.

7. Recommendations for Future Research

Electron emission spectroscopy under an applied field has recently been integrated to the UPS/TES system with a modified sample holder system. The new system is shown schematically in Fig.7.1(a). With this system, the TES, UPS and FES could be measured at the same time to more completely understand the electron emission and transport properties.

Fig.7.1 (b) shows a thermionic-field emission energy distribution diagram that could be obtained from the system. Field emission originates due to the tunneling of electrons with energies at or near the Fermi level. Thermionic emission originates from the vacuum level for most materials and the conduction band for semiconductors with negative electron affinity. In this system voltage supplies V_1 and V_2 are used to align the relative energy positions of the analyzer, grid and sample. The analyzer was kept at ground potential, and a constant voltage V_1 (-10V<-5V) is used to adjust the vacuum level of analyzer below the Fermi level of the sample. The variable voltage V_2 is used to induce field emission from the sample. The emission current can also be monitored in-situ using an Ampere meter behind the cathode emitter, shown in the Fig.7.1 (a), when there is thermionic/field emission.

This system for field enhanced UPS/TES/FES can be employed to study the energy distribution of vacuum electron emission from N/S-doped CVD diamond, carbon nanotubes and other materials. Additionally, this system could be used to investigate the band structure transition of VO_2 when there is Mott transition due to the temperature or field effect.

Thin film structures with N-doped CVD diamond have been developed in our laboratory which exhibit a 1.5 eV work function. In contrast, measurements of N-

doped single crystal diamond shows a 3.3eV work function which has been attributed to a large band bending effect[1]. It appears that the presence of the sp^2 bonded carbon in the CVD films helps reduce the band bending effects, but the NEA effects are still evident. Consequently it is necessary to further investigate the details of the effect of sp^2-related composition, structure and impurities on the band bending at surface.

For surfaces which exhibit field enhanced emission site, it is expected that application of a field will result in a lowering of the barrier (i.e. the Schottky effect). Moreover, surfaces with strong field enhancement factors due to the geometric effects should exhibit significant work function reduction which would be detected and confirmed by the FES/TES characterization.

Recently, reports have noted n-type diamond produced from P-doped CVD diamond[2]. Measurements have indicated that the phosphorus donor level is at 0.55 eV[3] below the conduction band. If the band bending could be controlled by engineering the growth, structure and doping, it may be possible to realize a 0.5 eV work function material which would enable many electron emission applications.

III-nitride hexagonal pyramid structures have been grown on patterned substrates and these structures could result in enhanced electron emission due to the Schottky effect. The effect of field and temperature on the electron emission from AlGaN layers needs to be investigated using the newly developed FES/TES/UPS system. Considering the built in polarization in nitride semiconductors, it is necessary to more thoroughly explore the polarity effect at the interface of metal/semiconductors and semiconductor/semiconductor heterostructures.

Reference:

1 L. Diederich, O. M. Kuttel, P. Ruffieux, T. Pillo, P. Aebi, and L. Schlapbach, Surf. Sci. **417**, 41 (1998).

2 H. Kato, S. Yamasaki, and H. Okushi, Diam. Relat. Mat. **14**, 2007 (2005).

3 S. Koizumi, T. Teraji, and H. Kanda, Diam. Relat. Mat. **9**, 935 (2000).

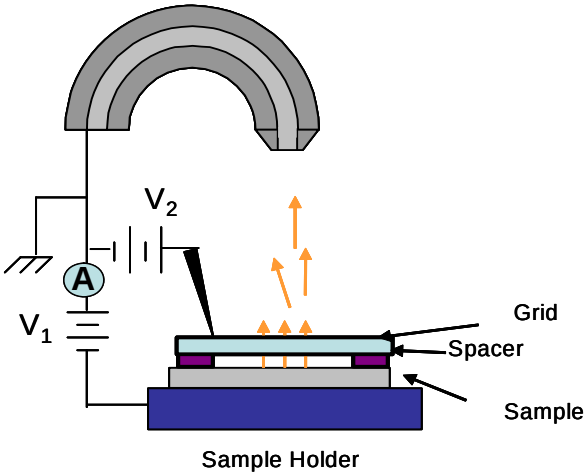

(a)

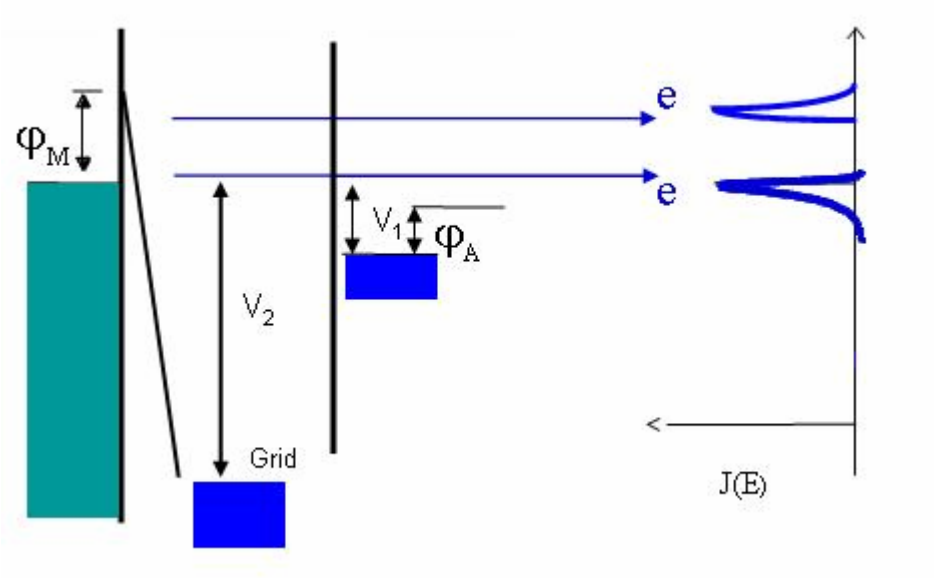

(b)

Figure 7.1 (a) System design of field emission spectroscopy (b) Field-thermionic emission energy distribution diagram. φ_M is the work function of the material and φ_A is the work function the analyzer.